The UbiB family member Cqd1 forms a novel membrane contact site in mitochondria

Siavash Khosravi[1], Xenia Chelius[2], Ann-Katrin Unger[2], Johanna Frickel[1], Timo Sachsenheimer[3], Christian Lüchtenborg[3], Rico Schieweck[1], Britta Brügger[3], Benedikt Westermann[2], Till Klecker[2], Walter Neupert[1,‡] and Max E. Harner[1]

[1] Department of Cell Biology, Biomedical Center, Medical Faculty, Ludwig-Maximilians University Munich, 82152 Planegg/Martinsried, Germany

[2] Institute of Cell Biology, University of Bayreuth, 95440 Bayreuth, Germany

[3] Heidelberg University Biochemistry Center (BZH), 69120 Heidelberg, Germany

[‡] Deceased

Running Title: The Cqd1-Por1-Om14 contact site

Key Words: Mitochondria, contact sites, UbiB protein family, phospholipids, mitochondrial biogenesis, mitochondrial morphology

Corresponding author: Max E. Harner

Mailing address: Großhaderner Str. 9, 82152 Planegg/Martinsried, Germany

Fax: +49 89 2180 75882

Phone: +49 89 2180 71885

e-mail address: max.harner@bmc.med.lmu.de

Summary statement

Here, we show that the conserved mitochondrial inner membrane protein Cqd1 interacts with the outer membrane proteins Por1 and Om14. Additionally, we provide evidence that Cqd1 is important for maintaining mitochondrial homeostasis.

Abstract

Mitochondria are essential organelles of eukaryotic cells that are characterized by their unique and complex membrane system. They are confined from the cytosol by an envelope consisting of two membranes. Signals, metabolites, proteins and lipids have to be transferred across these membranes via proteinaceous contact sites to keep mitochondria functional. In the present study we identified a novel mitochondrial contact site that is formed by the inner membrane protein Cqd1 and the outer membrane proteins Por1 and Om14. Similar to the mitochondrial porin, Por1, Cqd1 is highly conserved, suggesting that this complex is conserved in form and function from yeast to human. Cqd1 is a member of the UbiB protein kinase-like family (also called aarF domain containing kinases). It was recently shown that Cqd1 in cooperation with Cqd2 controls the cellular distribution of coenzyme Q by a yet unknown mechanism. Our data suggest that Cqd1 in addition is involved in the homeostasis of phospholipids and contributes to the maintenance of mitochondrial morphology and architecture.

Introduction

Mitochondria are essential organelles in eukaryotic cells and are characterized by an envelope consisting of two membranes. In addition to their important role in the cellular energy metabolism, mitochondria perform a multitude of other functions, including the synthesis of proteins, iron-sulfur clusters and lipids. Specialized structures in the mitochondrial membranes, so-called contact sites, have to be present to enable mitochondria to perform all these functions. The term contact site often refers to inter-organellar contacts, for instance between mitochondria and the endoplasmic reticulum (ER) (Kornmann et al., 2009; Murley et al., 2015), mitochondria and vacuoles, the yeast equivalent of mammalian lysosomes (Gonzalez Montoro et al., 2018; John Peter et al., 2017), or mitochondria and lipid droplets (Pu et al., 2011). In addition, intra-mitochondrial contact sites between the mitochondrial inner and outer membrane can be observed (Tamura et al., 2019). Importantly, both kinds of contacts are crucial for mitochondrial functions (Khosravi and Harner, 2020; Klecker et al., 2014; Kornmann, 2020; Phillips and Voeltz, 2016; Renne and Hariri, 2021).

Most contacts between the mitochondrial inner and outer membrane depend on the mitochondrial contact site and cristae organizing system (MICOS), a multi-subunit protein complex in the mitochondrial inner membrane (Harner et al., 2011; Hoppins et al., 2011; von der Malsburg et al., 2011). This highly conserved complex interacts with at least six different proteins or complexes of the outer membrane: the Fzo1-Ugo1 complex (Harner et al., 2011), the Miro GTPases (Modi et al., 2019), Om45 (Hoppins et al., 2011), Por1 (Hoppins et al., 2011), the TOB (SAM) complex (Bohnert et al., 2012; Darshi et al., 2011; Harner et al., 2011; Korner et al., 2012; Xie et al., 2007; Zerbes et al., 2012) and the TOM complex (Bohnert et al., 2012; von der Malsburg et al., 2011; Zerbes et al., 2012).

In addition, several other intra-mitochondrial contact sites exist that do not depend on MICOS. Some of these have been known for decades, like the TIM23-TOM super complex (Chacinska et al., 2003; Dekker et al., 1997; Schleyer and Neupert, 1985; Schwaiger et al., 1987), or the mitochondrial fusion machineries (Fritz et al., 2001; Sesaki et al., 2003; Wong et al., 2003). Others were identified just recently, for instance the contact site formed by Por1 (yeast porin) and Mdm31 that was suggested to be important for the biosynthesis of cardiolipin (Miyata et al., 2018). Apparently, the functions of these intra-mitochondrial contacts are quite diverse, varying from protein import to lipid transport and the formation of mitochondrial architecture and morphology.

Members of the poorly characterized UbiB protein kinase-like family (aarF domain containing kinases) were recently implicated in mitochondrial membrane homeostasis (Awad et al., 2020; Johnson et al., 2005; Kemmerer et al., 2021; Mollet et al., 2008; Odendall et al., 2019; Reidenbach et al., 2018; Stefely et al., 2015). UbiB family members are defined by the presence of a protein kinase-like domain (PKL) of unknown function. *Saccharomyces cerevisiae* has three family members which all reside in

79 mitochondria: Coq8 (Abc1), Cqd1 (Mco76) and Cqd2 (Mcp2) (Do et al., 2001; Morgenstern et al., 2017;
80 Tan et al., 2013). The bacterial proteins UbiB (*Escherichia coli*) and AarF (*Providencia stuartii*) are
81 essential for the synthesis of coenzyme Q (ubiquinone) (Macinga et al., 1998; Poon et al., 2000).
82 Likewise, Coq8 and its mammalian homolog ADCK3 are also part of the coenzyme Q biosynthesis
83 pathway (Do et al., 2001; Johnson et al., 2005; Mollet et al., 2008; Reidenbach et al., 2018; Stefely et
84 al., 2015). While our work was in progress, an elegant study linked also Cqd1 and Cqd2 to coenzyme Q
85 homeostasis. Deletion of *CQD1* results in excess export of coenzyme Q to extra-mitochondrial
86 membranes, whereas deletion of *CQD2* leads to an accumulation of excess coenzyme Q in
87 mitochondria. Thus, Cqd1 and Cqd2 apparently perform antagonistic roles in the distribution of
88 coenzyme Q between mitochondria and other organelles (Kemmerer et al., 2021).
89 In the present study, we set out to functionally analyze the conserved mitochondrial protein encoded
90 by the ORF *YPL109C*, which is now named Cqd1. We identified a MICOS-independent contact site
91 formed by Cqd1 in the mitochondrial inner membrane and Por1 and Om14 in the outer membrane.
92 Our characterization of the Δ*cqd1* deletion mutant suggests that Cqd1 contributes to phospholipid
93 homeostasis in addition to its role in the regulation of the distribution of coenzyme Q. Moreover, we
94 obtained evidence that defined levels of Cqd1 are important for mitochondrial morphology and
95 architecture.
96
97

98 ## Results

99 **Cqd1 is a mitochondrial inner membrane protein facing the intermembrane space**
100 We first asked where Cqd1 is precisely located within mitochondria. *In silico* analysis using MitoProt II
101 (Claros and Vincens, 1996) revealed that Cqd1 contains a potential N-terminal mitochondrial targeting
102 sequence (MTS; amino acids 1-15) (Fig. 1A) (SACS MEMSAT2 Transmembrane Prediction (Jones et al.,
103 1994)). In addition, a predicted transmembrane segment (amino acids 125-141) can be identified (Fig.
104 1A). We used an epitope-tagged construct (Cqd1-3xHA) to analyze the topology of Cqd1. Proteinase K
105 (PK) accessibility and alkaline extraction assays using isolated mitochondria showed that it is behaving
106 like Tim50 which is anchored in the inner membrane with an α-helical transmembrane domain (Fig. 1B
107 and C). PK did not degrade Cqd1-3xHA in intact mitochondria, but the signal was largely gone when PK
108 was added to hypotonically swollen mitochondria with a disrupted outer membrane. No shorter
109 fragment appeared upon addition of PK to swollen mitochondria indicating that the C-terminal tag was
110 degraded (Fig. 1B). Furthermore, Cqd1-3xHA remained in the pellet fraction upon alkaline extraction
111 like the membrane proteins Tom70 and Tim50 (Fig. 1C). It should be noted that in Western blot
112 analyses Cqd1-3xHA showed an apparent size of 66 kDa, instead of its calculated molecular weight of

76 kDa (untagged Cqd1 full length) or 74 kDa (untagged Cqd1 minus MTS) (Fig. 1B and C). We conclude that Cqd1 is present in the mitochondrial inner membrane with its major C-terminal part facing the intermembrane space.

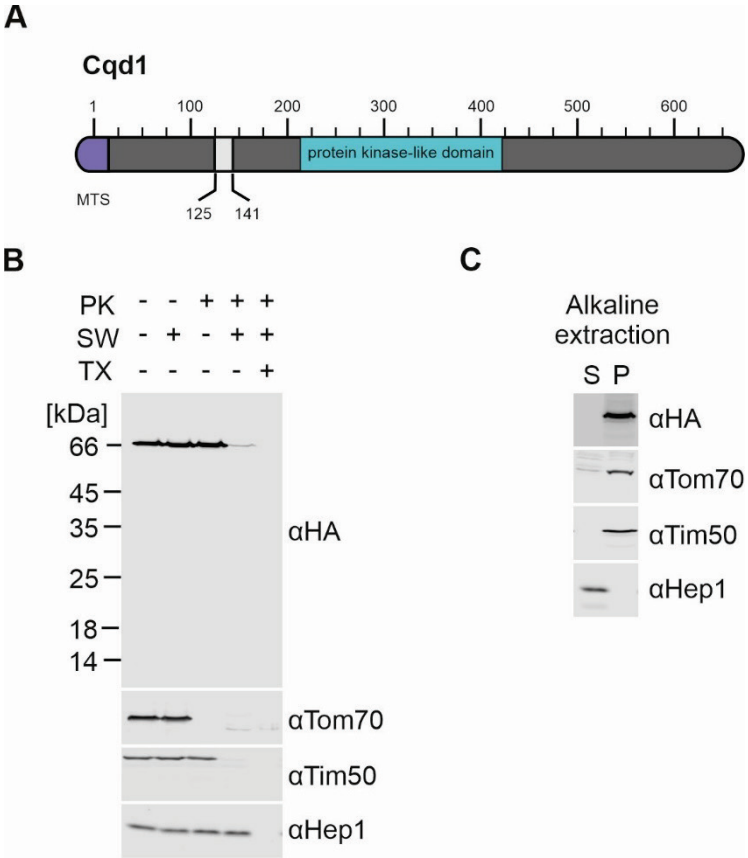

Figure 1. **Cqd1 is a mitochondrial inner membrane protein exposing its C-terminus to the intermembrane space.** **(A)** Schematic representation of Cqd1. Violet, mitochondrial targeting sequence (MTS; amino acids 1-15); light grey, predicted transmembrane domain (amino acids 125-141); turquoise, conserved protein kinase-like domain (amino acids 213-421). **(B)** Cqd1 exposes its C-terminus to the intermembrane space. Mitochondria isolated from a Cqd1-3xHA expressing strain were treated with isotonic buffer, subjected to swelling by incubation in hypotonic buffer to disrupt the outer membrane (SW), or lysed using a Triton X-100 containing buffer (TX). Proteinase K (PK) was added as indicated. Samples were analyzed by SDS-PAGE and immunoblotting. Tom70 was used as a marker for the outer membrane, Tim50 for the inner membrane and Hep1 for the matrix. **(C)** Cqd1 is an integral membrane protein. Isolated mitochondria were subjected to alkaline extraction to separate soluble and membrane proteins. Soluble proteins present in the supernatant (S) and membrane proteins in the pellet (P) were analyzed by SDS-PAGE and immunoblotting.

The *CQD1* gene negatively interacts with *UPS1* and *CRD1*

Several high-throughput screens showed that cells lacking Cqd1 are able to grow on non-fermentable carbon sources (Qian et al., 2012; Stenger et al., 2020). Also, Kemmerer et al. (2021) observed growth of Δ*cqd1* cells under respiratory conditions in liquid media, albeit growth was reduced when coenzyme Q precursors were depleted. We generated a deletion mutant lacking Cqd1 and analyzed its growth phenotype under several conditions on agar plates. We observed that the Δ*cqd1* mutant grows like

134 wild type on fermentable and non-fermentable carbon sources at normal and elevated temperatures
135 (Fig. 2A) confirming that Cqd1 is not essential for respiratory growth.
136 Mitochondria are intensively involved in the cellular phospholipid metabolism as they generate
137 cardiolipin and phosphatidylethanolamine. Interestingly, two independent high-throughput studies
138 revealed a genetic interaction of *CQD1* with *UPS1* (Costanzo et al., 2016; Hoppins et al., 2011). Ups1 is
139 responsible for transport of phosphatidic acid across the intermembrane space (Fig. 2B) (Connerth et
140 al., 2012; Tamura et al., 2012). Thus, we generated double deletion mutants lacking *CQD1* and genes
141 encoding proteins involved in mitochondrial phospholipid metabolism, including *CLD1*, *CRD1*, *GEP4*,
142 *MDM35*, *PGS1*, *PSD1*, *TAM41*, *TAZ1*, *UPS1* and *UPS2* (Fig. 2B). Growth analysis revealed a strong defect
143 of the double deletion mutant Δ*cqd1* Δ*ups1* specifically on synthetic medium (Fig. 2C). A weaker yet
144 reproducible growth defect at 37°C could be detected for the double deletion mutant Δ*cqd1* Δ*crd1*. All
145 other double deletion mutants did not show an enhanced growth phenotype. The growth defect of
146 the single deletion mutants Δ*tam41* and Δ*pgs1* was so strong that we cannot judge whether the
147 additional deletion of *CQD1* further reduces cell growth (Fig. 2C).
148 Cqd1 is a member of the highly conserved UbiB family (Kemmerer et al., 2021; Stefely et al., 2015) and
149 thus shows a predicted protein kinase-like domain (amino acids 213-421, Saccharomyces Genome
150 Database, SGD (Cherry et al., 2012)) (Fig. 1A). Therefore, we asked whether the protein kinase-like
151 domain of Cqd1 is important for its function. We generated mutants in conserved amino acid residues
152 within this domain (K275A, D288A and E330A) to inhibit ATP binding similar to what was done before
153 in studies on Cqd2 and Coq8 (Odendall et al., 2019; Reidenbach et al., 2018; Stefely et al., 2015). Of
154 note, introduction of the point mutations K275A or D288A led to strongly reduced steady state levels
155 of Cqd1 indicating reduced expression or stability of the protein (Fig. 2D). Therefore, we did not further
156 analyze these alleles. In contrast, the introduction of the point mutation E330A did not affect the
157 steady state level of Cqd1 (Fig. 2D). While expression of wild type Cqd1 largely restored the growth of
158 the double deletion mutant Δ*cqd1* Δ*ups1*, the *cqd1(E330A)* allele did not, indicating that ATP binding
159 of Cqd1 is important for its function (Fig. 2E). These results are in accordance with observations
160 recently made by Kemmerer et al. (2021) who reported that alleles carrying mutations of conserved
161 residues of the kinase-like domain were unable to rescue Δ*cqd1* growth defects.
162 In sum, we could manually confirm the negative genetic interaction of *CQD1* and *UPS1* and identified
163 *CRD1* as a novel negative interactor of *CQD1*. Interestingly, both genetic interactors are involved in
164 biosynthesis of the phospholipid cardiolipin. Furthermore, Cqd1 activity depends on an intact protein
165 kinase-like domain.
166

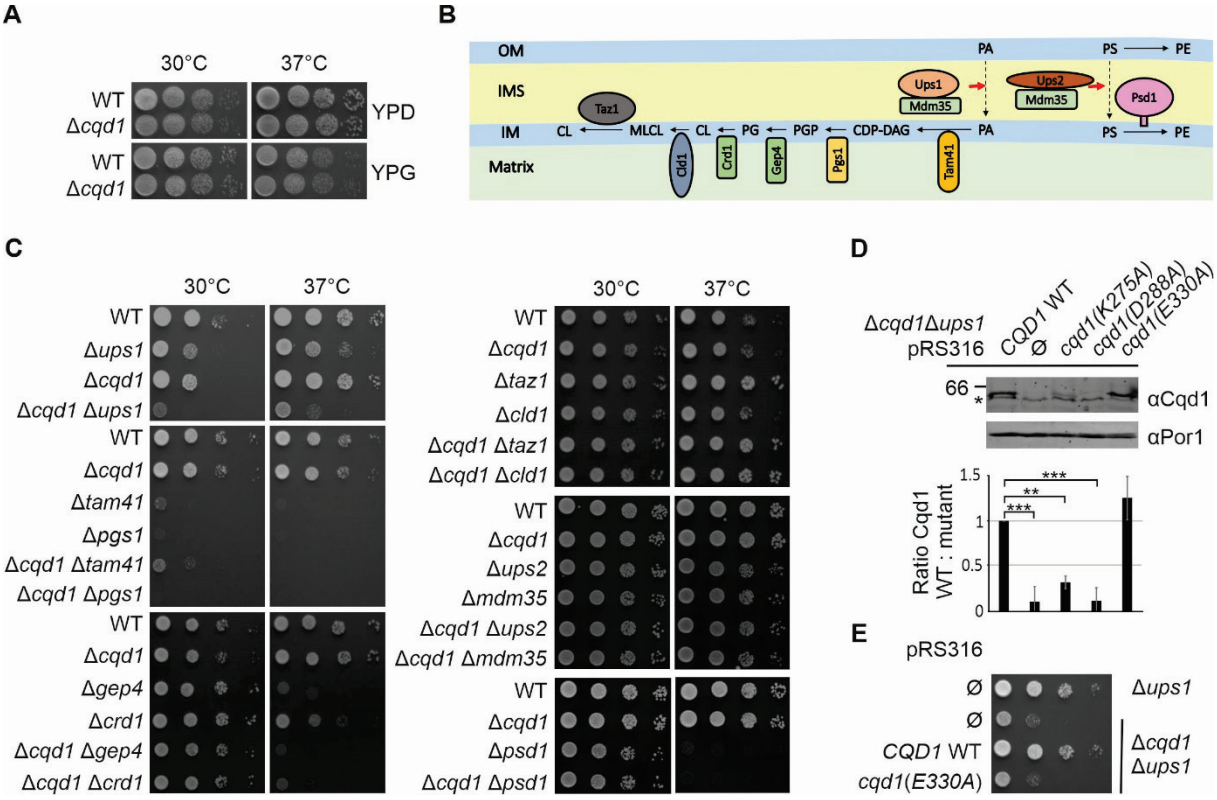

Figure 2. *CQD1* is a negative genetic interactor of *UPS1* and *CRD1*.

(A) Deletion of *CQD1* does not result in a growth defect. Cells of wild type and a Δ*cqd1* deletion strain were grown to logarithmic growth phase in rich medium containing glucose as carbon source (YPD). Cell growth was analyzed by drop dilution assay on plates containing rich medium supplemented with either glucose (YPD) or glycerol (YPG) at 30°C or 37°C. **(B)** Schematic illustration of the mitochondrial phospholipid metabolism. OM, outer membrane; IMS, intermembrane space; IM, inner membrane; PA, phosphatidic acid; CDP-DAG, cytidine diphosphate diacylglycerol; PGP, phosphatidylglycerol phosphate; PG, phosphatidylglycerol; CL, cardiolipin; MLCL, monolysocardiolipin; PS, phosphatidylserine; PE, phosphatidylethanolamine. **(C)** Deletion of *CQD1* from cells lacking Ups1 or Crd1 results in a synthetic growth defect. Cells were treated as in (A) with the difference that they were shifted to synthetic medium containing glucose (SCD) 30 h before growth analysis on SCD plates. **(D)** The conserved amino acids K275 and D288 in the predicted protein kinase-like domain are important for the stability of Cqd1. Cells bearing either the empty plasmid (Ø) or plasmids carrying the respective *cqd1* alleles were grown in SCGal. Crude mitochondria were isolated and the Cqd1 levels were analyzed by immunoblotting using an anti-Cqd1 antibody. (Upper panel) Immunodecorations of one representative experiment. The asterisk indicates a cross reaction of the anti-Cqd1 antibody. (Lower panel) Quantitative analysis of Cqd1 steady state level in the different strains analyzed in three independent experiments. Quantification was done using Image Studio software. Error bars indicate standard deviation. Asterisks represent p-values calculated by one-way ANOVA with subsequent Tukey's multiple comparison test (**p≤0.01; ***p≤0.001). **(E)** Glutamic acid 330 is essential for the function of Cqd1. Cells bearing either the empty plasmid or a plasmid carrying *CQD1* wild type (WT) or *cqd1(E330A)* alleles were treated as in (C).

Cqd1 contributes to mitochondrial lipid homeostasis

Next, we analyzed the phospholipid composition of mitochondria isolated from wild type yeast, the Δ*ups1* or Δ*cqd1* single deletion strains and the Δ*cqd1* Δ*ups1* double deletion mutant by mass

186 spectrometry. Consistent with previous results (Connerth et al., 2012), deletion of *UPS1* resulted in a
187 severe reduction of cardiolipin and monolysocardiolipin (Fig. 3, Suppl. Table 1). Also, we observed a
188 significant reduction of phosphatidic acid in Δ*ups1*, which might depend on growth conditions (Eiyama
189 et al., 2021). Interestingly, the lipidomics analysis of mitochondria obtained from Δ*cqd1* revealed a
190 significant reduction of phosphatidic acid while other phospholipids remained unchanged (Fig. 3,
191 Suppl. Table 1). The double deletion mutant Δ*cqd1* Δ*ups1* did not show a synthetic phenotype. We
192 suggest that Cqd1 is involved not only in maintenance of mitochondrial coenzyme Q levels (Kemmerer
193 et al., 2021), but also modulates the levels of phosphatidic acid (Fig. 3, Suppl. Table 1).

194
195
196
197
198
199
200

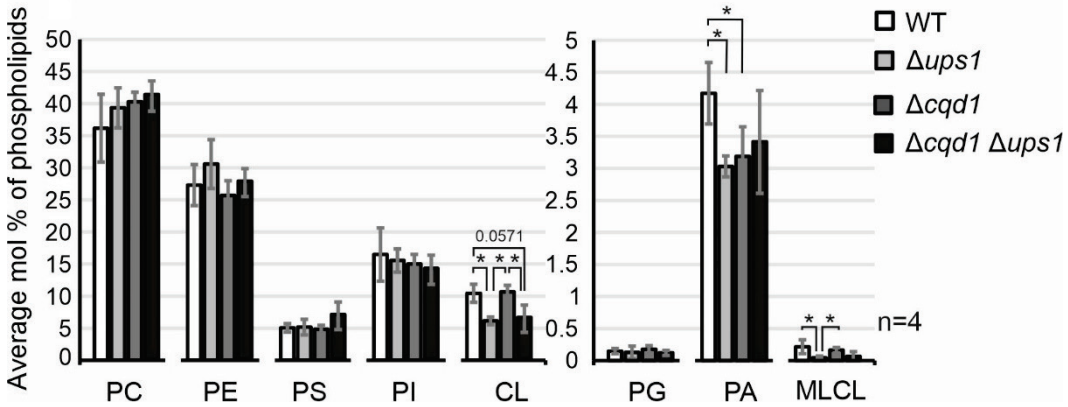

Figure 3. Cqd1 is involved in mitochondrial phospholipid homeostasis.

Strains were grown in synthetic medium containing glycerol (SCG) and mitochondria were purified by sucrose gradient centrifugation. Phospholipids were extracted and analyzed by mass spectrometry. The level of each phospholipid species (% of total phospholipids) is shown as a mean of four independently performed experiments with standard deviation bars. Asterisks represent p-values obtained by Mann Whitney test (*p≤0.05). PC, phosphatidylcholine; PE, phosphatidylethanolamine; PS, phosphatidylserine; PI, phosphatidylinositol; CL, cardiolipin; PG, phosphatidylglycerol; PA, phosphatidic acid; MLCL, monolysocardiolipin.

201

202 **Mitochondrial biogenesis and dynamics are impaired in the Δ*cqd1* Δ*ups1* double mutant**

203 The drastic growth phenotype of the Δ*cqd1* Δ*ups1* double mutant suggests that this strain struggles
204 with severe problems in essential mitochondrial functions which might be caused by a lack of
205 mitochondrial proteins or complexes involved in mitochondrial dynamics, architecture, protein import
206 and/or respiration. Therefore, we analyzed the steady state levels of various proteins involved in these
207 processes, including Fzo1, Ugo1, Mic27, Mic60, Tim23, Tim50, Rip1 and Cor2. Also, we tested assembly
208 of the TOM complex and the respiratory chain super complexes by native gel electrophoresis.
209 However, a comparison of the Δ*cqd1* Δ*ups1* double mutant with wild type and the single deletion
210 mutants revealed no significant defects (Fig. 4A and B).

211 Previous studies showed that deletion of *UPS1* compromises two processes that both depend on the
212 mitochondrial membrane potential. First, the import of the mitochondrial matrix-localized chaperone
213 Mdj1 is impaired resulting in the accumulation of unprocessed precursor (Tamura et al., 2009). And

second, processing of Mgm1, a large inner membrane-associated GTPase required for mitochondrial fusion, is reduced resulting in the accumulation of the long isoform, l-Mgm1 (Sesaki et al., 2006). Interestingly, deletion of *CQD1* did neither affect the import of Mdj1 nor processing of Mgm1. However, we found that both defects observed in the Δ*ups1* single mutant are exacerbated in the Δ*cqd1* Δ*ups1* double mutant. We observed a strong accumulation of Mdj1 precursor protein and an almost complete inhibition of Mgm1 processing (Fig. 4C and D). Previous studies showed that a balanced ratio of processed s-Mgm1 to unprocessed l-Mgm1 is necessary for mitochondrial fusion (DeVay et al., 2009; Zick et al., 2009). Accordingly, we observed a wild type like mitochondrial network in the Δ*cqd1* single deletion mutant. In the Δ*cqd1* Δ*ups1* double deletion mutant, however, the mitochondrial network appeared almost completely fragmented, indicating impairment of mitochondrial fusion (Fig. 4E). Thus, the relative mild phenotypes of the Δ*ups1* single deletion mutant regarding cell growth, generation of membrane potential and morphology of mitochondria (Sesaki et al., 2006; Tamura et al., 2009) are enhanced by additional deletion of the *CQD1* gene.

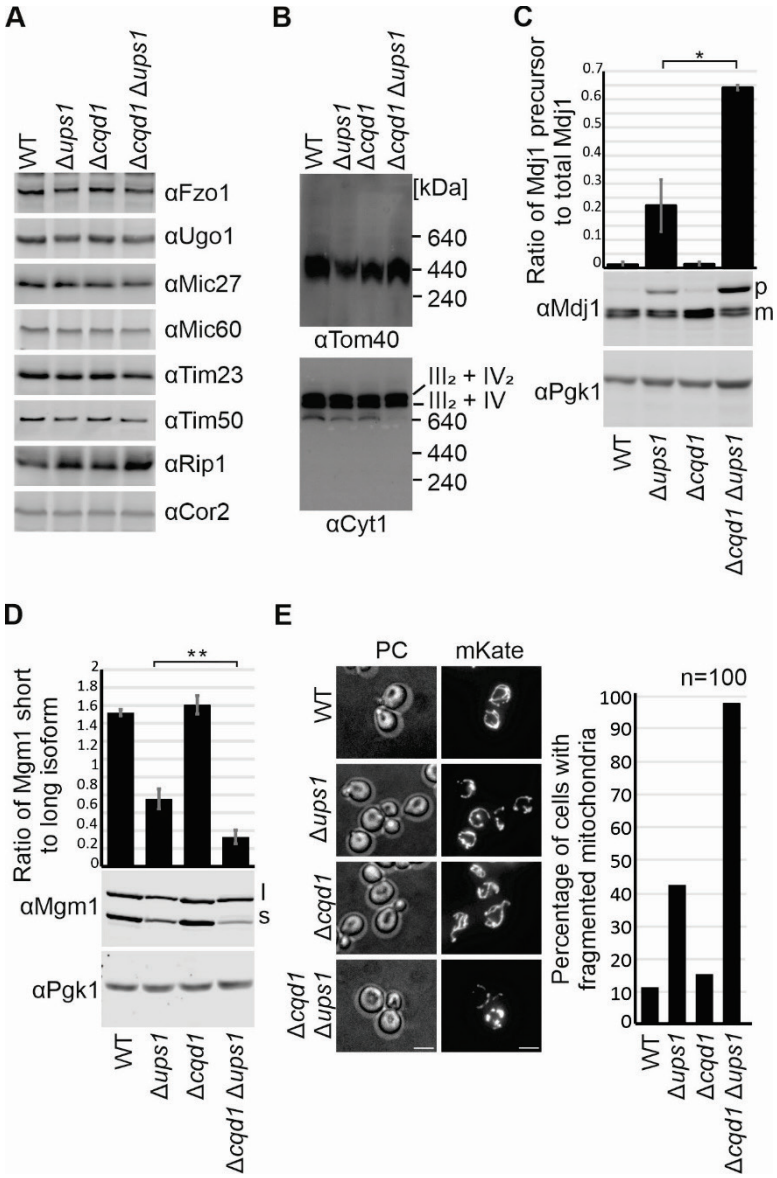

Figure 4. Simultaneous deletion of *CQD1* and *UPS1* impairs mitochondrial protein import and dynamics.

(A) Analysis of steady state levels of mitochondrial proteins in wild type cells and cells lacking Ups1, Cqd1, or both. Cells were grown in synthetic complete medium containing galactose (SCGal), and whole cell extracts were analyzed by immunoblotting. **(B)** Formation of mitochondrial protein complexes. Strains were grown in SCG. Isolated mitochondria were lysed in digitonin-containing buffer (3% w/v) and cleared lysates were subjected to BN-PAGE. The assembly of the TOM complex and respiratory chain super complexes were analyzed by immunoblotting using antibodies against Tom40 or Cyt1. **(C)** Deletion of *CQD1* in cells lacking Ups1 exacerbates accumulation of the precursor of Mdj1. Cells were grown in SCD, whole cell lysates were prepared and analyzed by immunoblotting with specific antibodies. Pgk1 served as a loading control. p, precursor of Mdj1; m, mature form of Mdj1. The quantification was obtained from three independent experiments and shows means of the ratio of the Mdj1 precursor to the total amount of Mdj1. Quantification was done using Image Studio software. Error bars indicate standard deviation. Asterisk represents p-value obtained by unpaired Student's t test (*p≤0.05). **(D)** Simultaneous deletion of *CQD1* and *UPS1* leads to strongly reduced processing of Mgm1. Whole cell lysates from cells grown in SCD were analyzed by immunoblotting. l, long isoform of Mgm1; s, short isoform of Mgm1. The quantification was obtained from three independent experiments and shows means of the ratio of the short form to the long form of Mgm1. Quantification was done using Image Studio software. Asterisks represent p-values obtained by unpaired Student's t test (**p≤0.01). **(E)** Mitochondria in cells lacking Ups1 and Cqd1 are highly fragmented. Mitochondria were labeled by expression of mKate targeted to mitochondria. Cells were grown in YPD and shifted to SCD, harvested in their logarithmic growth phase and immobilized on slides covered with concanavalin A. Scale bars, 4 µm. PC, phase contrast. For quantification 100 cells were counted for each strain.

249

250 **Cqd1 and Cqd2 have antagonistic roles in mitochondrial biogenesis**

251 A previous study indicated opposing functions of Cqd1 and Cqd2 (Kemmerer et al., 2021). Therefore,
252 we generated all possible single, double and triple deletion mutants to analyze the interaction network
253 of *CQD1*, *CQD2* and *UPS1*. Strikingly, growth analysis of the triple deletion mutant Δ*cqd1* Δ*ups1* Δ*cqd2*
254 revealed that deletion of *CQD2* in the Δ*cqd1* Δ*ups1* background completely rescued the growth
255 phenotype (Fig. 5A). At the same time, the accumulation of Mdj1 precursor protein and the impaired
256 Mgm1 processing were largely rescued (Fig. 5B and C). This suggests that the equilibrium of the
257 putative kinases Cqd1 and Cqd2 is particularly important when mitochondrial membrane lipid
258 composition is disturbed through deletion of *UPS1*.

259

260 **Cqd1 is part of a MICOS-independent contact site**

261 Our results described above and the observations reported by Kemmerer et al. (2021) suggest that
262 Cqd1 is involved in mitochondrial lipid homeostasis. We reasoned that a membrane contact site would
263 be ideally suited for such a function. To test whether Cqd1 is a contact site protein, we used an
264 established method to fractionate mitochondria, which is based on sonication, dounce
265 homogenization and subsequent density gradient centrifugation of mitochondrial particles (Harner et
266 al., 2011). Strikingly, Western blot analysis of mitochondrial fractions revealed that the distribution of
267 Cqd1 is clearly distinguishable from both the outer membrane marker Tom40 and the inner membrane
268

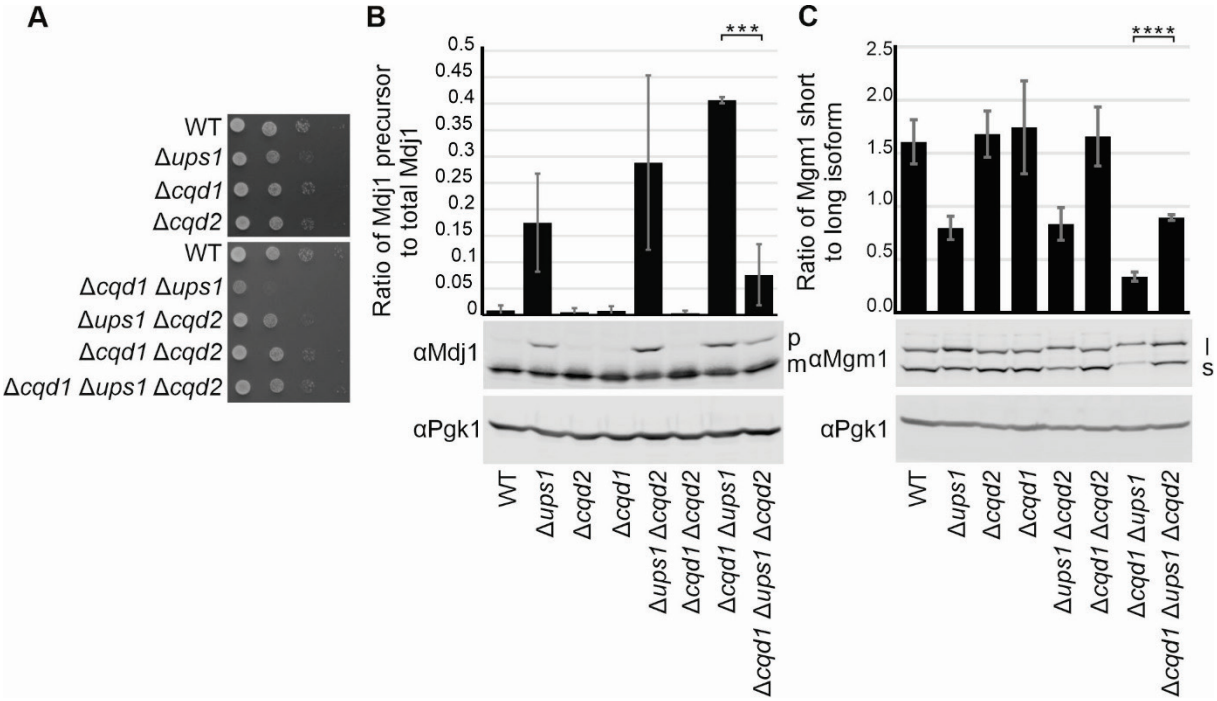

Figure 5. Deletion of *CQD2* restores the phenotypes of a Δ*cqd1* Δ*ups1* double deletion.

(A) Deletion of *CQD2* in the Δ*cqd1* Δ*ups1* background rescues the growth phenotype. Strains were grown to logarithmic phase and growth was analyzed by drop dilution assay on SCD plates at 30°C. **(B+C)** Mdj1 import and Mgm1 processing is restored in the Δ*cqd1* Δ*ups1* Δ*cqd2* triple mutant. Cells were grown in SCD, whole cell lysates were prepared and analyzed by immunoblotting. Pgk1 served as a loading control. **(B)** p, precursor of Mdj1; m, mature form of Mdj1. The quantification (Image Studio software) was obtained from three independent experiments and shows means of the ratio of the Mdj1 precursor to the total amount of Mdj1. **(C)** l, long isoform of Mgm1; s, short isoform of Mgm1. The quantification (Image Studio software) was obtained from three independent experiments and shows means of the ratio of the short form to the long form of Mgm1. Error bars indicate standard deviation. Asterisks represent p-values obtained by unpaired Student's t test (***p≤0.001; ****p≤0.0001).

marker Tim17. Cqd1 was enriched in fractions of intermediate density very similar to the MICOS subunit Mic27 (Fig. 6A and Suppl. Fig. 1).

In order to analyze whether Cqd1 is a novel MICOS subunit we performed immunoprecipitation of Cqd1 and different MICOS subunits. Neither the isolation of Cqd1 resulted in co-isolation of the MICOS subunits Mic10 or Mic60 nor vice versa (Fig. 6B and C). Native gel electrophoresis revealed that Cqd1 is present in a high molecular weight complex of ca. 400 kDa, a size that is clearly different from the 1.5 MDa large MICOS complex (Fig. 6D). These results suggest that Cqd1 is part of a novel contact site rather than a new MICOS subunit.

To screen for possible interaction partners of Cqd1 we first tested whether it might interact homotypically. To this end a yeast strain was generated expressing simultaneously a 3xHA-tagged and a 3xMyc-tagged version of Cqd1. Immunoprecipitation of Cqd1-3xHA led to efficient co-isolation of Cqd1-3xMyc, revealing homotypic interactions of Cqd1 (Fig. 6E).

283 While the homotypic Cqd1 interaction could explain the formation of the high molecular weight
284 complex (Fig. 6D), it does not explain the presence of Cqd1 in contact site fractions (Fig. 6A). Therefore,
285 chemical crosslinking was used to get an indication of further interaction partners. While incubation
286 with Di(N-succinimidyl) glutarate (DSG) did not reveal any crosslink partners, treatment with m-
287 maleimidobenzoyl-N-hydoxysuccinimide ester (MBS) produced two prominent crosslinks (Fig. 6F).
288 These two crosslink products of about 80 and 100 kDa indicated interaction partners with a molecular
289 weight of about 15 and 30 kDa. We identified Om14 and Por1, two highly abundant proteins forming
290 a complex in the mitochondrial outer membrane (Lauffer et al., 2012; Sakaue et al., 2019), as promising
291 candidates. Consistently, immunoprecipitation of Om14-3xHA allowed the co-isolation of Cqd1 and
292 Por1 (Fig. 6G) and Cqd1 was co-isolated upon immunoprecipitation of Por1-3xHA (Fig. 6H). The co-
293 isolation efficiency of Cqd1 was even higher than the co-isolation efficiency of Om45, a previously
294 identified interaction partner of Por1 in the outer membrane (Lauffer et al., 2012; Sakaue et al., 2019;
295 Wenz et al., 2014). Of note, we were not able to co-purify Por1 by isolating Cqd1-3xHA (Fig. 6B)
296 indicating that immunoprecipitation of Cqd1 impacts the integrity of the complex. Interestingly, Por1
297 was recently shown to form a contact site with the mitochondrial inner membrane protein Mdm31
298 (Miyata et al., 2018). Therefore, it might be that Cqd1 is a novel subunit of this complex. However,
299 isolation Mdm31-3xHA did not result in co-isolation of Cqd1 (our unpublished observations).
300 Most of the so far identified contact sites between the mitochondrial inner and outer membranes
301 depend on MICOS (Bohnert et al., 2012; Darshi et al., 2011; Harner et al., 2011; Hoppins et al., 2011;
302 Korner et al., 2012; Modi et al., 2019; von der Malsburg et al., 2011; Xie et al., 2007; Zerbes et al.,
303 2012). In particular, Mic60 is essential for the integrity of the MICOS complex as well as the formation
304 of MICOS-dependent contact sites (Harner et al., 2011; Hoppins et al., 2011; von der Malsburg et al.,
305 2011). Although we did not detect a physical interaction between Cqd1 and MICOS, the interaction of
306 Cqd1 with Por1 and Om14 might still depend on the presence of an intact MICOS complex. To test this,
307 we performed immunoprecipitation of Om14-3xHA expressed in the wild type background or the
308 Δ*mic60* deletion background. We observed that immunoprecipitation of Om14-3xHA led to the
309 successful co-isolation of Cqd1 and Por1 independent of the presence of Mic60 (Fig. 6I).
310 Taken together, we identified a novel contact site formed by the mitochondrial inner membrane
311 protein Cqd1 and the previously described Por1-Om14 complex in the mitochondrial outer membrane
312 (Lauffer et al., 2012; Sakaue et al., 2019). This new contact site exists independently of contact sites
313 formed by MICOS.
314
315

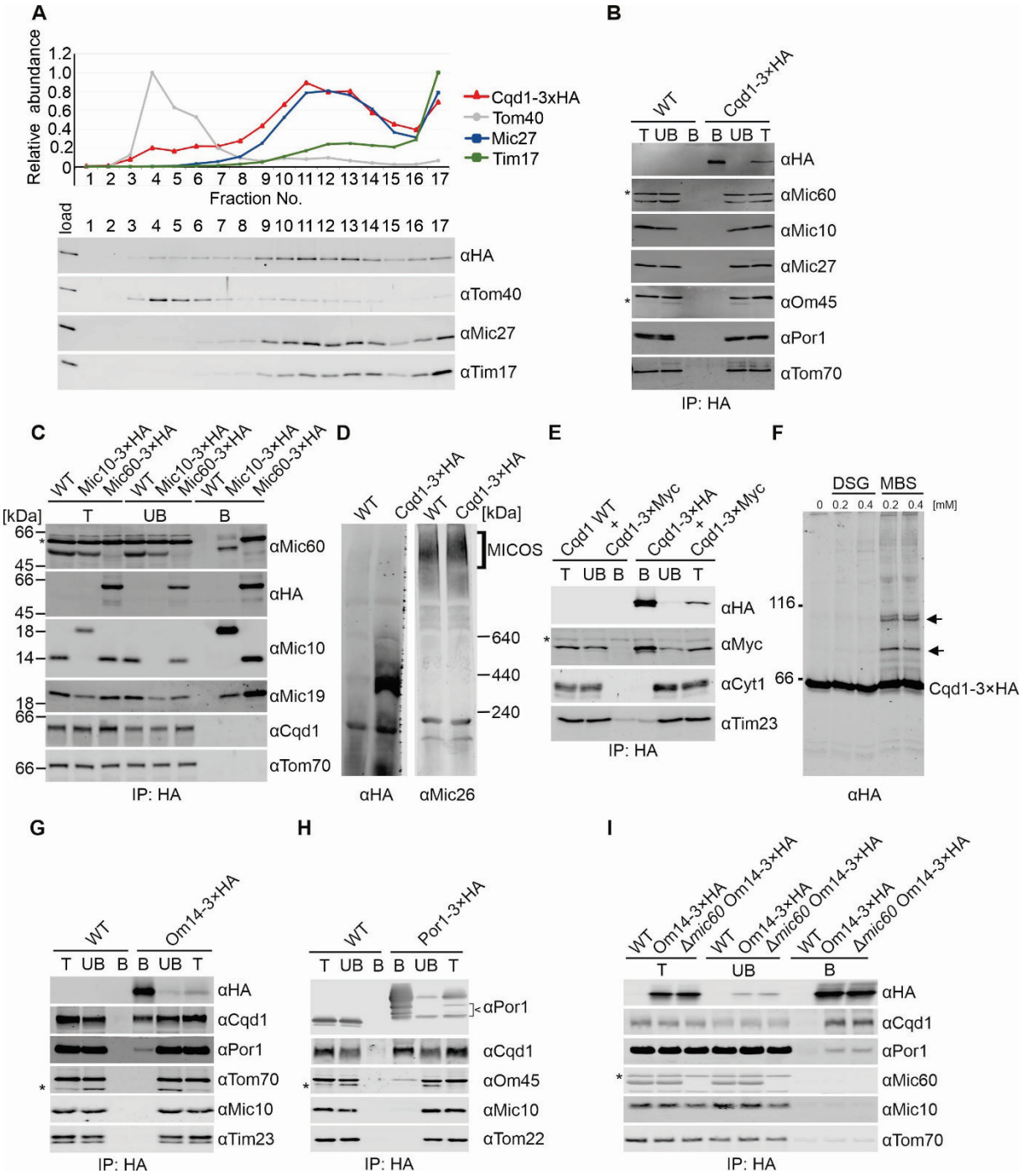
A
Relative abundance
Fraction No.
Cqd1-3xHA
Tom40
Mic27
Tim17
load
αHA
αTom40
αMic27
αTim17
B
WT
Cqd1-3×HA
T UB B B UB T
αHA
αMic60
αMic10
αMic27
αOm45
αPor1
αTom70
IP: HA
C
WT
Mic10-3×HA
Mic60-3×HA
[kDa]
T
UB
B
αMic60
αHA
αMic10
αMic19
αCqd1
αTom70
IP: HA
D
WT
Cqd1-3×HA
[kDa]
MICOS
640
440
240
αHA
αMic26
E
Cqd1 WT + Cqd1-3×Myc
Cqd1-3×HA + Cqd1-3×Myc
T UB B B UB T
αHA
αMyc
αCyt1
αTim23
IP: HA
F
DSG
MBS
0 0.2 0.4 0.2 0.4 [mM]
116
66
Cqd1-3×HA
αHA
G
WT
Om14-3×HA
T UB B B UB T
αHA
αCqd1
αPor1
αTom70
αMic10
αTim23
IP: HA
H
WT
Por1-3×HA
T UB B B UB T
αPor1
αCqd1
αOm45
αMic10
αTom22
IP: HA
I
WT
Om14-3×HA
Δmic60 Om14-3×HA
T
UB
B
αHA
αCqd1
αPor1
αMic60
αMic10
αTom70
IP: HA

Figure 6. Cqd1 forms a novel contact site with Om14 and Por1.

(A) Cqd1 is enriched in contact site fractions. Mitochondria of a Cqd1-3xHA expressing strain were isolated, subjected to osmotic shrinking, sonication, and sucrose density gradient centrifugation. The gradient was fractionated, proteins were subjected to TCA precipitation and analyzed by immunoblotting. (Top) The graph shows mean values of three independent experiments for the distribution of Cqd1-3xHA and the marker proteins for the outer membrane (Tom40), the inner membrane (Tim17) or contact sites (Mic27). Error bars indicating standard deviations are shown in Suppl. Fig. 1. (Bottom) Immunodecorations of one representative experiment. **(B)** Mic10 and Mic60 do not co-precipitate with Cqd1. Mitochondria of wild type and a yeast strain expressing Cqd1-3xHA were isolated and lysed in digitonin containing buffer (1% w/v). Lysates were subjected to immunoprecipitation using anti-HA affinity agarose. The indicated fractions were analyzed by SDS-PAGE and immunoblotting. T, total lysate (5%); UB, unbound protein (5%); B, bound protein (100%). Asterisks indicate cross reactions of the antibodies against Mic60 or Om45. **(C)** Cqd1 does not co-precipitate with Mic10 or Mic60. Mitochondria of wild type or yeast strains expressing Mic10-3xHA or Mic60-3xHA were analyzed as in (B). T, total lysate (2.5%); UB, unbound protein (2.5%); B, bound protein (100%). The asterisk indicates a cross reaction of the anti-Mic60 antibody. Since the cross reaction of the Mic60 antibody shows the same size as Mic60-3xHA, a decoration of this membrane fragment with an anti-HA antibody is presented additionally. **(D)** Cqd1 forms high molecular weight complexes. Mitochondria isolated from wild type and a yeast strain expressing Cqd1-3xHA were solubilized in digitonin (3% w/v). Cleared lysates were subjected to BN-PAGE. Cqd1-3xHA containing complexes were detected by immunoblotting with an anti-HA antibody. Analysis of the MICOS complex using an anti-Mic26 antibody served as control. **(E)** Cqd1 interacts homotypically. Mitochondria of yeast strains expressing Cqd1-3xMyc in the presence of untagged or 3xHA tagged Cqd1 were treated as described in (B). T, total lysate (5%); UB, unbound protein (5%); B, bound protein (100%). The asterisk indicates a cross reaction of the anti-Myc antibody. **(F)** Cqd1 interacts with other proteins than itself. Isolated mitochondria of a Cqd1-3xHA expressing strain were exposed to DMSO or the chemical crosslinkers DSG and MBS at the indicated concentrations. Samples were analyzed by immunoblotting with an anti-HA antibody. Arrows indicate Cqd1-containing crosslinks. **(G)** Cqd1 interacts with Om14. Mitochondria of wild type and a yeast strain expressing Om14-3xHA were analyzed as in (B). T, total lysate (2.5%); UB, unbound protein (2.5%); B, bound protein (100%). The asterisk indicates a cross reaction of the anti-Tom70 antibody. **(H)** Cqd1 interacts with Por1. Mitochondria of wild type or a yeast strain expressing Por1-3xHA were analyzed as in (B). T, total lysate (1%); UB, unbound protein (1%); B, bound protein (100%). The arrowhead indicates degradation products of Por1-3xHA. The asterisk indicates a cross reaction of the anti-Om45 antibody. **(I)** The contact site formed by Cqd1 and Om14 is independent of MICOS. Mitochondria of wild type, Om14-3×HA and Δ*mic60* Om14-3×HA strains were analyzed as in (B). T, total lysate (2.5%); UB, unbound protein (2.5%); B, bound protein (100%). The asterisk indicates a cross reaction of the anti-Mic60 antibody.

351

352 **Overexpression of *CQD1* leads to altered mitochondrial architecture and morphology**

353 Cells overexpressing *CQD1* from the strong *GAL* promoter showed a dramatically reduced growth rate
354 (Fig. 7A). Western blot analysis using a Cqd1 specific antibody revealed the appearance of a slower
355 migrating band, probably representing the accumulation of some Cqd1 precursor protein, upon
356 overexpression (Fig. 7B, arrowhead). The levels of several other mitochondrial proteins involved in
357 mitochondrial dynamics, protein import, mitochondrial architecture or respiration were not changed
358 compared to wild type and the Δ*cqd1* deletion mutant (Fig. 7B). However, when we analyzed the
359 presence of different mitochondrial protein complexes, we found that monomeric and dimeric F_1F_O

360 ATP synthase complexes were strongly reduced. In contrast, respiratory chain super complexes were
361 not significantly changed (Fig. 7C).
362 The F_1F_O ATP synthase is essential for the establishment of mitochondrial inner membrane architecture
363 (Klecker and Westermann, 2021). Absence of assembled, dimeric F_1F_O ATP synthase results in the
364 formation of septa that cross the matrix completely or onion-like structures (Davies et al., 2012;
365 Habersetzer et al., 2013; Harner et al., 2016; Paumard et al., 2002; Rabl et al., 2009). Therefore, we
366 asked whether the lack of assembled F_1F_O ATP synthase complexes in the *CQD1* overexpression strain
367 results in altered mitochondrial architecture. The Δ*cqd1* deletion strain appeared like wild type also in
368 electron micrographs, whereas overexpression of *CQD1* led to massively distorted mitochondrial
369 membrane architecture in many cells (Fig. 7D, Suppl. Fig. 2). Mitochondria were often aggregated into
370 huge clusters and we frequently observed loss of normal cristae, in many cases accompanied by the
371 formation of elongated inner membrane structures (Fig. 7D, arrow, Suppl. Fig. 2). Thus, aberrant
372 mitochondrial architecture upon overexpression of Cqd1 complements the loss of assembled F_1F_O ATP
373 synthase.
374 Furthermore, in several cases we noticed membraneous structures within these clusters that might
375 represent ER membranes (Fig. 7D, arrowheads, Suppl. Fig. 2). To test this, we simultaneously analyzed
376 the morphology of mitochondria and the ER by fluorescence microscopy in wild type and the *CQD1*
377 deletion and overexpression strains. When *CQD1* was overexpressed mitochondria in most cells did
378 not appear as the characteristic tubular network that is spread all over the cell, but instead formed
379 swollen clusters (Fig. 7E and F, Suppl. Fig. 3). Remarkably, these clusters indeed contained a large
380 proportion of ER membranes (Fig. 7E).
381 In summary, overexpression of *CQD1* causes severe phenotypes on growth, assembly of the F_1F_O ATP
382 synthase, and mitochondrial architecture and morphology. Interestingly, the effect of overexpression
383 of the inner membrane protein Cqd1 is apparently not only restricted to the inner membrane but also
384 affects inter-organellar contacts.
385
386
387

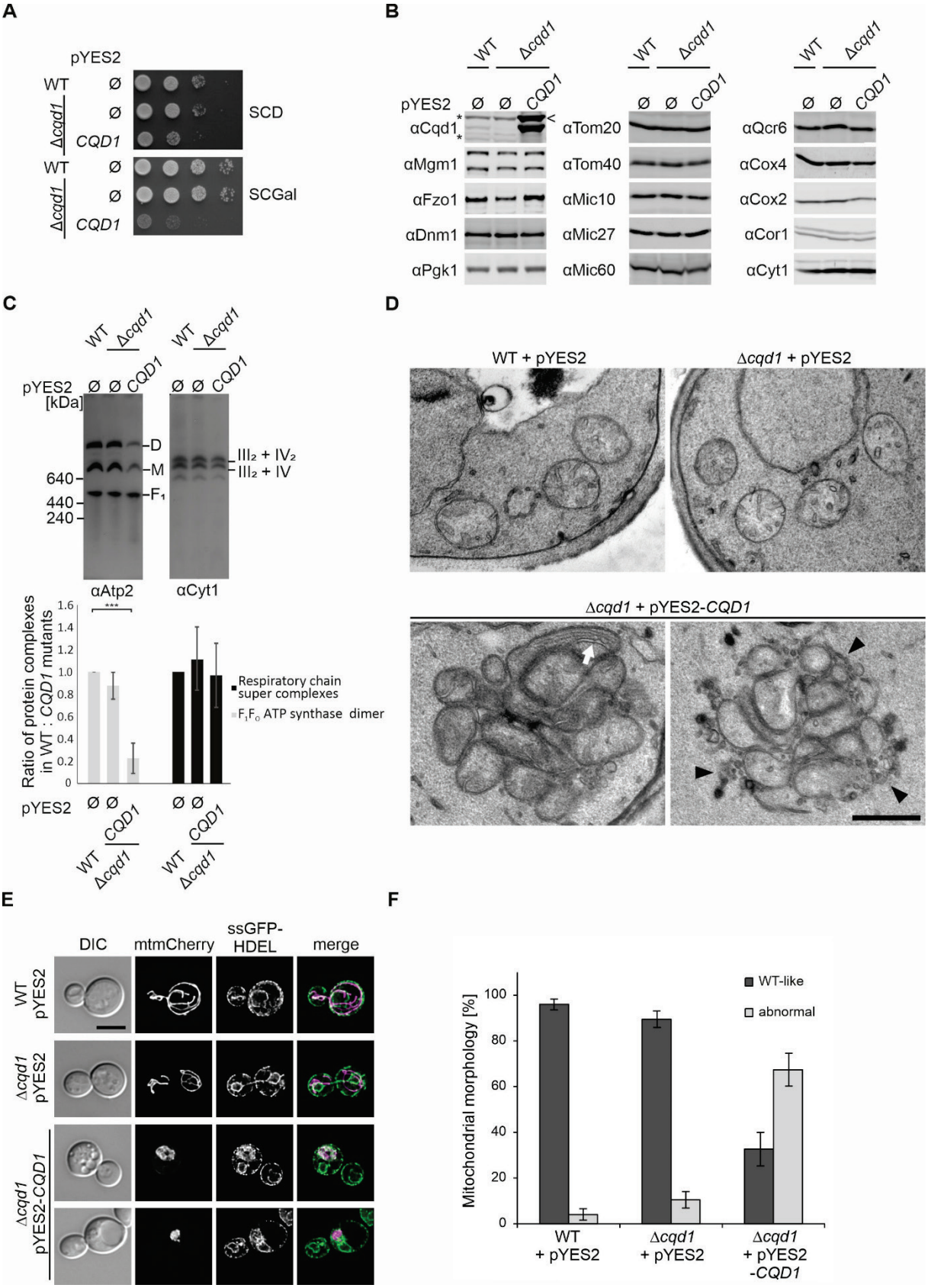
A
pYES2
WT
Δcqd1
Ø
Ø
CQD1
SCD
SCGal
B
WT
Δcqd1
pYES2
Ø
CQD1
αCqd1
αMgm1
αFzo1
αDnm1
αPgk1
αTom20
αTom40
αMic10
αMic27
αMic60
αQcr6
αCox4
αCox2
αCor1
αCyt1
C
[kDa]
640
440
240
D
M
F₁
III₂ + IV₂
III₂ + IV
αAtp2
αCyt1
***
Ratio of protein complexes in WT : CQD1 mutants
Respiratory chain super complexes
F₁F₀ ATP synthase dimer
D
WT + pYES2
Δcqd1 + pYES2
Δcqd1 + pYES2-CQD1
E
DIC
mtmCherry
ssGFP-HDEL
merge
WT pYES2
Δcqd1 pYES2
Δcqd1 pYES2-CQD1
F
Mitochondrial morphology [%]
WT-like
abnormal
WT + pYES2
Δcqd1 + pYES2
Δcqd1 + pYES2 -CQD1

388

389

Figure 7. Overexpression of *CQD1* leads to dramatic changes in architecture and morphology of mitochondria.
(A) Overexpression of *CQD1* is toxic. Wild type and Δ*cqd1* cells carrying an empty vector (pYES2) and Δ*cqd1* cells expressing *CQD1* from a high-copy plasmid with a galactose-inducible promoter (pYES2-*CQD1*) were grown in SCD and shifted to SCGal prior to analysis. **(B)** Deletion or overexpression of *CQD1* does not affect steady state levels of mitochondrial proteins. Whole cell extracts of wild type and yeast cells in which *CQD1* was deleted or overexpressed were analyzed by immunoblotting. Asterisks indicate cross reactions of the anti-Cqd1 antibody. The arrowhead indicates the potential precursor form of Cqd1. **(C)** Overexpression of Cqd1 results in strongly reduced levels of assembled F_1F_O ATP synthase. Isolated mitochondria of cells grown in SCGal were lysed in buffer containing digitonin (3% w/v) and cleared lysates were subjected to BN-PAGE. The assembly of the F_1F_O ATP synthase or the respiratory chain super complexes was analyzed by immunoblotting using antibodies against Atp2 or Cyt1. D, dimer of the F_1F_O ATP synthase; M, monomer of the F_1F_O ATP synthase; F_1, F_1 subcomplex of the F_1F_O ATP synthase. (Upper panel) Immunodecorations of one representative experiment are shown. (Lower panel) Quantification of signal intensities of the F_1F_O ATP synthase dimers and the respiratory chain super complexes (complex III dimer - complex IV monomer and complex III dimer - complex IV dimer) present in the indicated strains of three independent experiments were done with Image J software. Error bars indicate standard deviation. Asterisks represent p-values calculated by one-way ANOVA with subsequent Tukey's multiple comparison test (***$p \leq 0.001$). **(D)** Overexpression of *CQD1* results in highly altered mitochondrial architecture. Cells were grown overnight in SCGal, subjected to chemical fixation with glutaraldehyde and osmium tetroxide, embedded in Epon, and ultrathin sections were analyzed by transmission electron microscopy. The white arrow highlights elongated inner membrane structures, black arrowheads highlight membranes presumably representing cross-sections of ER tubules. Scale bar, 500 nm. Additional electron micrographs are shown in Suppl. Fig. 2. **(E)** Overexpression of *CQD1* leads to the formation of mitochondria-ER clusters. Strains expressing mitochondria-targeted mCherry (mtmCherry) and ER-targeted GFP (ssGFP-HDEL) were grown to logarithmic growth phase in SCGal, fixed with formaldehyde, and examined by deconvolution fluorescence microscopy. Shown are maximum intensity projections of z stacks of entire cells (mitochondria) or of the center of the cells (ER, four consecutive z sections). DIC, *differential interference contrast.* Scale bar, 5 µm. **(F)** Strains expressing mitochondria-targeted GFP were analyzed as in (E) and mitochondrial morphology was quantified. Columns represent mean values from two independent experiments with three biological replicates per strain and at least 150 cells per replicate, error bars indicate standard deviation. Representative images are shown in Suppl. Fig. 3.

390

391 # Discussion

392 In the present study, we characterized the highly conserved protein kinase-like domain containing
393 protein Cqd1. All members of the UbiB family present in yeast, Cqd1, Cqd2 and Coq8, participate in
394 coenzyme Q metabolism (Do et al., 2001; Johnson et al., 2005; Kemmerer et al., 2021; Reidenbach et
395 al., 2018; Stefely et al., 2015; Subramanian et al., 2019; Xie et al., 2012). In contrast to the Δ*coq8,*
396 mutant deletion of *CQD1* does not result in reduced production but affects distribution of coenzyme
397 Q within the cellular membrane system (Kemmerer et al., 2021). The molecular role of Cqd1 in this
398 process is unknown so far. However, membrane contacts would be ideally suited to facilitate the
399 transition of these hydrophobic molecules (Kemmerer et al., 2021). The key finding of our study, the

400 contact site formed by Cqd1, Por1 and Om14, is in good agreement with this hypothesis. Based on our
401 results indicating that Cqd1 is also involved in phospholipid homeostasis, it is tempting to speculate
402 that it might contribute to the import of phosphatidic acid, and possibly other lipids, into the inner
403 membrane in addition to its role in coenzyme Q distribution.
404 We consider it unlikely that Cqd1 itself is a lipid transporter, as the absence of Cqd1 leads to increased
405 export of coenzyme Q rather than block of transport (Kemmerer et al., 2021). However, it is
406 conceivable that Cqd1 has an accessory or regulatory role and interacts with additional, yet unknown
407 interaction partners in the inner membrane. This idea would be in line with models of other lipid
408 transport systems, like the bacterial maintenance of lipid asymmetry (Mla) pathway first identified in
409 *E. coli* (Malinverni and Silhavy, 2009). Here, the MlaFEDB complex is involved in the ATP-dependent
410 transport of lipids between the bacterial inner and outer membranes (Malinverni and Silhavy, 2009;
411 Thong et al., 2016). This complex is composed of the canonical proteins MlaE and MlaF and the
412 auxiliary proteins MlaB and the hexameric MlaD in the inner membrane, and cooperates with MlaC, a
413 soluble protein in the periplasm, and the outer membrane protein MlaA (Ekiert et al., 2017; Malinverni
414 and Silhavy, 2009; Thong et al., 2016). Intriguingly, MlaA interacts with the porins OmpC and OmpF
415 (Chong et al., 2015) and it was proposed that it works in both directions between the bacterial
416 membranes (Ekiert et al., 2017; Malinverni and Silhavy, 2009). The Mla pathway represents a transport
417 system based on transient protein interactions, in contrast to the here discovered permanent contact.
418 However, it shares two striking features with Cqd1: an interaction with porin across two membranes
419 and the regulation of bi-directional lipid transport.
420 In addition to the observed changes in phospholipid composition upon deletion of *CQD1*,
421 overexpression of *CQD1* results in altered mitochondrial architecture. These changes are characterized
422 by the formation of huge mitochondrial clusters and aberrant inner membrane structures. We and
423 others observed similar alterations of inner membrane structure when analyzing yeast mutants lacking
424 dimeric F_1F_O ATP synthase (Davies et al., 2012; Harner et al., 2016; Paumard et al., 2002; Rabl et al.,
425 2009). And indeed, overexpression of *CQD1* goes along with a strong reduction of assembled F_1F_O ATP
426 synthase. Furthermore, we observed that mitochondrial clusters intimately interact with ER
427 membranes. This suggests that Cqd1 might have a function in mitochondrial architecture that goes
428 beyond regulation of coenzyme Q and phosphatidic acid homeostasis. It remains a challenge for the
429 future to reveal the molecular mechanisms in this process.
430
431

432 ## Material and Methods

433 **Yeast strains and cell growth**

434 *S. cerevisiae* YPH499 was used as wild type (WT). Chromosomal manipulations (knockouts, C-terminal
435 3xHA and 3xMyc tagging) were performed according to established procedures (Knop et al., 1999;
436 Longtine et al., 1998). For the generation of deletion strains, the entire coding regions of the
437 corresponding genes were replaced by the indicated marker cassettes. Double mutant strains were
438 also generated by homologous recombination. The genotypes of the strains used in this study are listed
439 in Supplementary Table 2.

440 For the generation of pRS316-*CQD1,* pRS316-*CQD1*-3xHA and pYES2-*CQD1* plasmids, the coding region
441 of *CQD1* was amplified by PCR. The intron present in the *CQD1* open reading frame was removed when
442 cloning the initial pYES2 construct. This construct served as template DNA for cloning of pRS316-*CQD1*.
443 The coding region of *CQD1*-3xHA was amplified from yeast genomic DNA of the *CQD1*-3xHA strain.
444 *CQD1*-3xHA was cloned under control of its endogenous promoter and the *ADH1* terminator into the
445 pRS316 vector by enzymatic assembly of overlapping DNA fragments (Gibson, 2011). The point
446 mutations K275A, D288A, and E330A in *CQD1* were introduced into pRS316-*CQD1* by site directed
447 mutagenesis. For the generation of the pYX142-ssGFP-HDEL plasmid the *Sac*I/*Eco*RI fragment of
448 pYX122-ssGFP-HDEL (Bockler and Westermann, 2014) was ligated into the *Sac*I/*Eco*RI sites of pYX142-
449 mtGFP (Westermann and Neupert, 2000). The primers used in this study are listed in Supplementary
450 Table 3.

451 Yeast cells were grown as indicated on YP medium supplemented with 2% glucose (YPD) or 3% glycerol
452 (YPG) or synthetic medium supplemented with 2% glucose (SCD), 3% galactose (SCGal) or 3% glycerol
453 (SCG) (Izawa and Unger, 2017).

454 Growth of the different strains was analyzed by the drop dilution assay. Cells were grown and kept in
455 logarithmic growth phase, washed with water, diluted in water to an OD_{600} of 0.5 and serial dilutions
456 were prepared (1:10; 1:100; 1:1,000). 5 µl of each dilution were spotted on agar plates with the
457 indicated media. All strains without plasmids were grown initially in YPD liquid medium for 16 h. For
458 analysis of cell growth on YP medium, cells were harvested after growth in YPD. When growth on
459 synthetic medium was analyzed, cells were shifted from YPD to SCD 30 h prior to analysis. Cell carrying
460 pYES2 plasmids were grown initially in SCD liquid medium for 16 h and shifted to SCGal for 7h before
461 growth was analyzed.

462

463 **Whole cell extract**

464 Whole cell extracts were prepared as described previously (Kushnirov, 2000). In brief, cells were grown
465 in the indicated media to exponential growth phase (OD_{600} 0.5 - 1.0) and an equivalent of cells

466 corresponding to 2.5 OD_{600} was collected by centrifugation. Harvested cells were resuspended in 200 µl
467 of 0.1 M NaOH and incubated at room temperature for 5 min. Cell pellets were resuspended in 50 µl
468 of SDS sample buffer and analyzed by SDS-PAGE and immunoblotting.
469
470 **Isolation of crude mitochondria**
471 Cells were grown at 30°C in SCD, SCG, SCGal or YPG as indicated. Mitochondria were isolated by
472 differential centrifugation as described previously (Izawa and Unger, 2017) with slight modifications.
473 In brief, cells were harvested and washed with distilled water. Cells were treated for 10 min with DTT
474 (10 mM final concentration) followed by treatment with zymolyase (200 U per gram wet weight of
475 cells) for 30 min at 30°C with gentle agitation. Sphaeroplasts were opened by repeated pipetting in
476 isotonic lysis buffer (20 mM MOPS-KOH pH 7.2, 1 mM EDTA, 0.6 M sorbitol, 0.2% (w/v) BSA, 1 mM
477 phenylmethylsulfonyl fluoride (PMSF)). Mitochondria were harvested after a clarifying spin at 2,000 ×g
478 and 4°C for 5 min by centrifugation at 14,000 ×g and 4°C for 10 min and resuspended in SM buffer (0.6
479 M sorbitol, 20 mM MOPS, pH 7.4).
480
481 **Sucrose gradient purification of mitochondria**
482 Crude mitochondria were isolated as described above except that the final mitochondrial pellet was
483 resuspended in 15 ml of buffer A (0.6 M Sorbitol, 50 mM MES pH 6.0) and re-isolated by centrifugation
484 for 10 min at 17,000 xg and 4°C. Crude mitochondria were resuspended in 2 ml of buffer A and 10 mg
485 were loaded on top of a sucrose step gradient (1.5 ml of 60%, 5 ml of 35%, 1.5 ml of 25%, and 1.5 ml
486 of 15% sucrose in buffer A). Mitochondria were separated from other organelles by ultracentrifugation
487 for 1 h at 134,000 xg and 4°C. Purified mitochondria were harvested from the boundary between 60%
488 and 35% sucrose layers, resuspended in 15 ml of SM buffer and re-isolated by centrifugation for 15
489 min at 14,000 xg and 4°C. Mitochondria were resuspended in SM buffer to a final concentration of 10
490 mg/ml.
491
492 **Subfractionation of mitochondria**
493 Vesicles consisting of pure mitochondrial outer membrane, mitochondrial inner membrane, and
494 vesicles consisting of both membranes were generated and separated as described before (Harner,
495 2017) with slight modifications. 10 mg of freshly isolated crude mitochondria were resuspended in 1.6
496 ml of SM buffer. Mitochondria were swollen by addition of 16 ml swelling buffer (20 mM MOPS pH
497 7.4) and subsequent incubation for 30 min at 4°C under mild stirring. Sucrose concentration was
498 adjusted to 0.55 M. Vesicles were generated by sonication (four times 30 seconds at 10% amplitude
499 intermitted by 30 seconds breaks). After a clarifying spin for 20 min at 20,000 ×g and 4°C, vesicles were
500 concentrated on the 2.5 M sucrose cushion by centrifugation at 118,000 ×g and 4°C for 100 min.

501 Concentrated vesicles were harvested and the suspension was homogenized by dounce
502 homogenization. Vesicles were separated by centrifugation for 12 hours at 200,000 ×g and 4°C through
503 a sucrose step gradient (0.8 M, 0.96 M, 1.02 M, 1.13 M, 1.25 M sucrose in 20 mM MOPS-KOH pH 7.4
504 and 0.5 mM EDTA). The gradient was harvested and proteins were subjected twice to trichloroacetic
505 acid precipitation (TCA; final concentration of 14.4%).
506
507 **Alkaline extraction**
508 100 µg of isolated mitochondria were diluted in SM buffer to a concentration of 1 mg/ml. An equal
509 volume of 200 mM sodium carbonate was added followed by an incubation on ice for 30 min.
510 Membrane and soluble proteins were separated by centrifugation for 30 min at 91,000 ×g and 4°C.
511 Proteins present in the supernatant were subjected to TCA precipitation. The membrane protein pellet
512 and the precipitated soluble proteins were resuspended in SDS sample buffer and analyzed by SDS-
513 PAGE and immunoblotting.
514
515 **Proteolytic susceptibility assay**
516 100 µg of mitochondria were incubated in SM buffer (0.6 M sorbitol, 20 mM MOPS, pH 7.4), swelling
517 buffer (20 mM MOPS, pH 7.4) or lysis buffer (1% (v/v) Triton X-100, 20 mM MOPS, pH 7.4) for 20 min
518 on ice. Proteinase K was added (final concentration of 0.2 mg/ml) as indicated and samples were
519 incubated on ice for 15 min. Proteolysis was stopped by addition of PMSF to a final concentration of 4
520 mM. Samples were centrifuged at 17,000 ×g and 4°C for 20 min. Pellets were resuspended in SM buffer
521 and subjected to TCA precipitation. Samples were analyzed by SDS-PAGE and immunoblotting.
522
523 **Blue native gel electrophoresis (BN-PAGE**)
524 150 µg (MICOS complex) or 50 µg (all other mitochondrial protein complexes) of isolated mitochondria
525 were resuspended in 15 µl (MICOS complex) or 50 µl (all other mitochondrial protein complexes) of
526 BN buffer (50 mM NaCl, 50 mM imidazole-HCl, 2 mM 6-aminohexanoic acid, 1 mM EDTA, 1 mM PMSF,
527 pH 7.0) (Wittig et al., 2006) supplemented with 3% digitonin. After a clarifying spin for 15 min at 14,000
528 ×g and 4°C 2 µl (MICOS complex) or 7 µl (all other mitochondrial protein complexes) G-250 Sample
529 Additive (Invitrogen, Waltham, Massachusetts, USA) containing 40% glycerol were added. Protein
530 complexes were separated on 3-12% NativePAGE Novex Bis-Tris gels (Invitrogen). Electrophoresis was
531 performed for 30 min at 150 V followed by 2 hours at 250 V. Proteins were transferred to PVDF
532 membrane by wet blotting for 2 hours at 30 mV.
533

534 **Chemical crosslinking**

535 Isolated mitochondria were diluted in 100 µl of SI buffer (50 mM HEPES-KOH, 0.6 M sorbitol, 75 mM
536 KCl, 10 mM $Mg(Ac)_2$, 2 mM KH_2PO_4, 2.5 mM EDTA, 2.5 mM $MnCl_2$, pH 7.2) to a concentration of 1
537 mg/ml. Disuccinimidyl glutarate (DSG) and m-maleimidobenzoyl-N-hydroxysuccinimide ester (MBS)
538 were added from freshly prepared stock solutions to the final concentration of 200 or 400 µM and
539 incubated on ice for 30 min. The reaction was stopped by the addition of glycine to a final
540 concentration of 100 mM followed by incubation on ice for 10 min. Mitochondria were re-isolated by
541 centrifugation at 17,000 xg and 4°C for 10 min. The pellets were resuspended in SDS sample buffer and
542 analyzed by SDS-PAGE and immunoblotting.

543

544 **Immunoprecipitation assay**

545 3 mg mitochondria (except for Cqd1-3×HA, 1 mg of mitochondria) were lysed in IP buffer (50 mM Tris-
546 HCl pH 7.4, 50 mM NaCl) containing 1% (w/v) digitonin and 1 mM PMSF. After a clarifying spin for 10
547 min at 12,000 xg and 4°C, lysates were incubated with anti-HA agarose beads (20 µl of beads per 1 mg
548 of proteins) (Merck, Darmstadt, Germany) for 2 h. Anti-HA agarose beads were washed 3 times with
549 500 µl IP buffer containing 0.1% (w/v) digitonin and 1 mM PMSF before and after incubation with
550 lysates. The indicated amount of total lysate and unbound material was taken, subjected to TCA
551 precipitation and resuspended in SDS sample buffer. Bound proteins were eluted with SDS sample
552 buffer at 95°C for 10 min. Fractions were analyzed by SDS-PAGE followed by immunoblotting.

553

554 **Fluorescence microscopy**

555 For visualizing mitochondria, the mitochondrial presequence of *Neurospora crassa* subunit 9 of the
556 F_1F_O ATP synthase was fused to mKate2. The nucleotide sequence was inserted into the HO locus of
557 the yeast genome and expressed constitutively under the control of the *PGK1* promoter. Yeast cells
558 were grown overnight in YPD at 30°C. The next day, cells were diluted in synthetic media containing
559 2% glucose and were kept in logarithmic phase for 24 hours. Cells corresponding to an OD_{600} of 1 were
560 harvested by centrifugation at 2,500 xg for 3 min. Cells were vortexed for 1 min and washed with 1 ml
561 of sterile 1x PBS. Cell pellets were resuspended in 200 µl 1x PBS and immobilized on µ-slides (Ibidi,
562 Gräfelfing, Germany) coated with 1 mg/ml of concanavalin A. After immobilizing, cells were covered
563 with 400 µl SCD medium. Microscopy was performed at 30°C on a Nikon Ti2-Eclipse microscope (Nikon,
564 Tokyo, Japan) equipped with a CFI Apochromat TIRF 100x/1.49 NA oil objective and a TwinCam LS dual
565 camera splitter attached to two Photometrics Prime 95B 25 mm cameras (Teledyne Photometrics,
566 Tucson, USA).

567 For visualization of mitochondria or mitochondria and the ER upon *CQD1* overexpression, strains
568 carried either pYX142-mtGFP (Westermann and Neupert, 2000) or pYX232-mtmCherry (Dirk Scholz,
569 University of Bayreuth) and pYX142-ssGFP-HDEL, respectively. Cells were grown overnight in
570 galactose-containing synthetic complete medium supplemented with 0.1% glucose, shifted to
571 galactose-containing synthetic complete medium without glucose, incubated until logarithmic growth
572 phase and fixed with 3.7% formaldehyde. Microscopy was performed using a Leica DMi8 fluorescence
573 microscope (Leica Microsystems GmbH, Wetzlar, Germany) equipped with a HC PL APO 100x/1.40 oil
574 objective, a Lumencor SPECTRA X light source and fluorescence filter sets (TXR Cube ex. 540-580 nm;
575 em. 592-668 nm and FITC Cube ex. 460-500 nm; em. 512-542 nm). Images were taken with a Leica
576 DFC9000 GT VSC-07400 sCMOS camera. For microscope settings, image generation, and processing
577 (cropping, maximum intensity projection), the Leica LAS X software (version 3.6.0.20104, Leica
578 Microsystems GmbH, Wetzlar, Germany) was used. For deconvolution of z stacks the Deconvolution
579 Software Huygens Essential (version 18.10, Scientific Volume Imaging, Hilversum, The Netherlands)
580 was used. For adjustment of brightness and contrast and the overlay of different channels Adobe
581 Photoshop CS6 (Adobe Systems) was used. For simultaneous analysis of the morphology of
582 mitochondria and the ER, z stacks were recorded with a z-step size of 213 nm. In the case of
583 mitochondria, maximum intensity projections of z stacks of entire cells are shown, whereas for the ER
584 maximum intensity projections of four consecutive z sections of the center of the cells are shown.
585
586 **Electron microscopy**
587 For electron microscopy, cells were first grown in synthetic complete medium containing glucose as
588 carbon source and then shifted to synthetic complete medium containing galactose as carbon source,
589 in which they were grown overnight. Chemical fixation of yeast cells with glutaraldehyde and osmium
590 tetroxide, dehydration, Epon embedding, and subsequent steps of sample preparation for electron
591 microscopy were performed as described previously (Unger et al., 2017). Electron micrographs were
592 taken with a JEOL JEM-1400 Plus transmission electron microscope operated at 80 kV, a JEOL Ruby
593 CCD camera (3296 x 2472 pixels), and the TEM Center software Ver.1.7.12.1984 or Ver.1.7.19.2439
594 (JEOL, Tokyo, Japan).
595
596 **Lipid analysis**
597 Lipidomics analyses were performed as described in Papagiannidis et al. (2021). Aliquots
598 corresponding to 1500-2000 pmol total lipid were subjected to acidic Bligh and Dyer extractions
599 performed in the presence of internal lipid standards from a master mix containing 40 pmol d_7-PC mix
600 (15:0/18:1-d7, Avanti Polar Lipids), 25 pmol PI (17:0/20:4, Avanti Polar Lipids), 25 pmol PE and 15 pmol
601 PS (14:1/14:1, 20:1/20:1, 22:1/22:1, semi-synthesized as described in Özbalci et al, 2013), 20 pmol PA

602 (PA 17:0/20:4, Avanti Polar Lipids) 5 pmol PG (14:1/14:1, 20:1/20:1, 22:1/22:1, semi-synthesized as
603 described in Ozbalci et al. (2013), 25 pmol CL 57:4 (14:1/14:1/14:1/15:1, Avanti Polar Lipids) and 25
604 pmol MLCL (16:0/16:0/16:0, Echelon). Lipids recovered in the organic extraction phase were
605 evaporated by a gentle stream of nitrogen. Prior to measurements, lipid extracts were dissolved in 10
606 mM ammonium acetate in methanol, diluted 1:10 and transferred into Eppendorf twin.tec 96-well
607 plates. Mass spectrometric measurements were performed in positive ion mode on an AB SCIEX QTRAP
608 6500+ mass spectrometer equipped with chip-based (HD-D ESI Chip, Advion Biosciences) nano-
609 electrospray infusion and ionization (Triversa Nanomate, Advion Biosciences) as described (Özbalci et
610 al, 2013). The following precursor ion scanning (PREC) and neutral loss scanning (NL) modes were used
611 for the measurement of the various lipid classes: +PREC 184 (PC), +NL141 (PE), +NL185 (PS), +NL277
612 (PI), +NL189 (PG), +NL115 (PA). Mass spectrometry settings: Resolution: unit, low mass configuration;
613 data accumulation: 400 MCA; curtain gas: 20; interface heater temperature: 60°C; CAD: medium. Data
614 evaluation was done using LipidView (Sciex) and ShinyLipids, a software developed in house. For MS
615 analysis of CL and MLCL, dried lipids were re-dissolved in 40% UPLC solvent B (90% 2-propanol/10%
616 acetonitrile/0.1% formic acid/10 mM NH_4HCO_3) and transferred to silanized glass inserts
617 (Phenomenex) using Hamilton syringes. The glass inserts were placed in Eppendorf tubes and
618 centrifuged in an Eppendorf centrifuge at 3000 rpm for 3 min. Lipid samples were then subjected to
619 UPLC-ESI-MS/MS analysis performed on an Ultimate® 3000 LC system (Dionex, Thermo Fisher
620 Scientific) coupled to a QExactive Hybrid Quadrupole-Orbitrap instrument (Thermo Scientific). For LC
621 separations, an ACQUITY UPLC CSH C18 1.7µm, 1.0 x 150 mm column (Waters) was used. The column
622 oven temperature was set to 55°C, the temperature of the autosampler was set to 20°C. The flow rate
623 used was 100 µl/min. The solvent composition used was as follows: 60% acetonitrile/40% H_2O/0.1%
624 formic acid/10 mM NH_4HCO_3 (solvent A), 90% 2-propanol/10% acetonitrile/0.1% formic acid/10 mM
625 NH_4HCO_2 (solvent B). The starting solvent composition was 50% solvent B/50% solvent A. The
626 conditions of the gradient were as follows: 7 min: 90% solvent B, 7-17 min: 90% solvent B, 17.1 min
627 50% solvent B and 17.1-25 min: 50% solvent B. The MS analyses were performed in the positive ion
628 mode. CL and MLCL species were measured as $[M+NH_4^+]$ ions. The following ESI source parameters
629 were used: sheath gas flow rate: 4 (a.u.), auxiliary gas flow rate: 0, sweep gas flow rate: 0, spray
630 voltage: 1.5 kV, capillary temperature: 200°C, S-lens RF level: 50. Full-MS scans were recorded using
631 the following parameters: resolution: 140,000 (at m/z 200) AGC-target: 1e6, maximum IT: 200 ms, scan
632 range: m/z 500-2000. Data evaluation was performed using MassMap.
633

634 **Statistics**

635 Statistics were calculated using the software GraphPad Prism (version 5; GraphPad, San Diego, CA,
636 USA). Mass spectrometry analysis was performed in quadruplicate. Data are represented as mean ±
637 standard deviation. For statistical analysis, data was first tested for normal distribution using Shapiro-
638 Wilk normality test. P-Values were calculated using Mann Whitney test. Analysis of Mdj1 precursor
639 accumulation and Mgm1 processing in the various yeast strains was performed in triplicate. Data are

640 represented as mean ± standard deviation. P-Values were calculated using an unpaired Student's t
641 test. Analysis of the steady state level of Cqd1 variants expressed from pRS316 under the control of
642 the endogenous Cqd promotor as well as the level of assembled mitochondrial protein complexes were
643 performed in triplicates. Data are represented as mean ± standard deviation. P-Values were calculated
644 using an one-way ANOVA test with subsequent Tukey's multiple comparison test. $p < 0.05$ was
645 considered statistically significant.

646

647 ## Acknowledgements

648 We thank Rita Grotjahn (University of Bayreuth) for help with electron microscopy. M.E.H. thanks Dr.
649 Christof Osman, Ludwig-Maximilians University, Munich, for providing his microscope and support.
650 M.E.H. is greatly thankful for the helpful discussion with Dr. Bill Wickner, Dartmouth Medical School,
651 Hanover. Furthermore, M.E.H. thanks Dr. Michael Kiebler, Ludwig-Maximilians, University, Munich, for
652 generous and extensive support.

653

654 ## Competing interests

655 The authors declare that there is no conflict of interest.

656

657 ## Funding

658 M.E.H. thanks the Jung-Stiftung für Wissenschaft und Forschung, the Friedrich-Baur-Stiftung (Reg.-Nr.
659 02-20), *LMUexcellent* and the Deutsche Forschungsgemeinschaft (DFG), project number 413985647
660 for financial support. B.B. was supported by the DFG, project number 112927078 - TRR 83, B.W. was
661 supported by the DFG, project number 433461293, T.K. was supported by the DFG, project number
662 459304237, and the Elitenetzwerk Bayern (ENB) through the Biological Physics program.

663

664 ## Author contributions

665 S.K., X.C., A.K.U, J.F., T.K., M.E.H., conception and design, acquisition of data, analysis and
666 interpretation of data, drafting or revising the article; T.S., C.L., R.S., acquisition of data, analysis and
667 interpretation of data, revising the article; B.B., B.W., W.N., conception and design, analysis and
668 interpretation of data, drafting or revising the article.

669

670

671 ## References

672 Awad, A.M., Nag, A., Pham, N.V.B., Bradley, M.C., Jabassini, N., Nathaniel, J., and Clarke, C.F. (2020).
673 Intragenic suppressor mutations of the COQ8 protein kinase homolog restore coenzyme Q biosynthesis
674 and function in Saccharomyces cerevisiae. PLoS One *15*, e0234192.
675 Bockler, S., and Westermann, B. (2014). Mitochondrial ER contacts are crucial for mitophagy in yeast.
676 Dev Cell *28*, 450-458.
677 Bohnert, M., Wenz, L.S., Zerbes, R.M., Horvath, S.E., Stroud, D.A., von der Malsburg, K., Muller, J.M.,
678 Oeljeklaus, S., Perschil, I., Warscheid, B.*, et al.* (2012). Role of mitochondrial inner membrane
679 organizing system in protein biogenesis of the mitochondrial outer membrane. Mol Biol Cell *23*, 3948-
680 3956.
681 Chacinska, A., Rehling, P., Guiard, B., Frazier, A.E., Schulze-Specking, A., Pfanner, N., Voos, W., and
682 Meisinger, C. (2003). Mitochondrial translocation contact sites: separation of dynamic and stabilizing
683 elements in formation of a TOM-TIM-preprotein supercomplex. EMBO J *22*, 5370-5381.
684 Cherry, J.M., Hong, E.L., Amundsen, C., Balakrishnan, R., Binkley, G., Chan, E.T., Christie, K.R., Costanzo,
685 M.C., Dwight, S.S., Engel, S.R.*, et al.* (2012). Saccharomyces Genome Database: the genomics resource
686 of budding yeast. Nucleic Acids Res *40*, D700-705.
687 Chong, Z.S., Woo, W.F., and Chng, S.S. (2015). Osmoporin OmpC forms a complex with MlaA to
688 maintain outer membrane lipid asymmetry in Escherichia coli. Mol Microbiol *98*, 1133-1146.
689 Claros, M.G., and Vincens, P. (1996). Computational method to predict mitochondrially imported
690 proteins and their targeting sequences. Eur J Biochem *241*, 779-786.
691 Connerth, M., Tatsuta, T., Haag, M., Klecker, T., Westermann, B., and Langer, T. (2012).
692 Intramitochondrial transport of phosphatidic acid in yeast by a lipid transfer protein. Science *338*, 815-
693 818.
694 Costanzo, M., VanderSluis, B., Koch, E.N., Baryshnikova, A., Pons, C., Tan, G., Wang, W., Usaj, M.,
695 Hanchard, J., Lee, S.D.*, et al.* (2016). A global genetic interaction network maps a wiring diagram of
696 cellular function. Science *353*.
697 Darshi, M., Mendiola, V.L., Mackey, M.R., Murphy, A.N., Koller, A., Perkins, G.A., Ellisman, M.H., and
698 Taylor, S.S. (2011). ChChd3, an inner mitochondrial membrane protein, is essential for maintaining
699 crista integrity and mitochondrial function. J Biol Chem *286*, 2918-2932.
700 Davies, K.M., Anselmi, C., Wittig, I., Faraldo-Gomez, J.D., and Kuhlbrandt, W. (2012). Structure of the
701 yeast F1Fo-ATP synthase dimer and its role in shaping the mitochondrial cristae. Proc Natl Acad Sci U
702 S A *109*, 13602-13607.
703 Dekker, P.J., Martin, F., Maarse, A.C., Bomer, U., Muller, H., Guiard, B., Meijer, M., Rassow, J., and
704 Pfanner, N. (1997). The Tim core complex defines the number of mitochondrial translocation contact
705 sites and can hold arrested preproteins in the absence of matrix Hsp70-Tim44. EMBO J *16*, 5408-5419.
706 DeVay, R.M., Dominguez-Ramirez, L., Lackner, L.L., Hoppins, S., Stahlberg, H., and Nunnari, J. (2009).
707 Coassembly of Mgm1 isoforms requires cardiolipin and mediates mitochondrial inner membrane
708 fusion. J Cell Biol *186*, 793-803.
709 Do, T.Q., Hsu, A.Y., Jonassen, T., Lee, P.T., and Clarke, C.F. (2001). A defect in coenzyme Q biosynthesis
710 is responsible for the respiratory deficiency in Saccharomyces cerevisiae abc1 mutants. J Biol Chem
711 *276*, 18161-18168.
712 Eiyama, A., Aaltonen, M.J., Nolte, H., Tatsuta, T., and Langer, T. (2021). Disturbed intramitochondrial
713 phosphatidic acid transport impairs cellular stress signaling. J Biol Chem *296*, 100335.
714 Ekiert, D.C., Bhabha, G., Isom, G.L., Greenan, G., Ovchinnikov, S., Henderson, I.R., Cox, J.S., and Vale,
715 R.D. (2017). Architectures of Lipid Transport Systems for the Bacterial Outer Membrane. Cell *169*, 273-
716 285 e217.
717 Fritz, S., Rapaport, D., Klanner, E., Neupert, W., and Westermann, B. (2001). Connection of the
718 mitochondrial outer and inner membranes by fzo1 is critical for organellar fusion. J Cell Biol *152*, 683-
719 692.
720 Gibson, D.G. (2011). Enzymatic assembly of overlapping DNA fragments. Methods Enzymol *498*, 349-
721 361.

722 Gonzalez Montoro, A., Auffarth, K., Honscher, C., Bohnert, M., Becker, T., Warscheid, B., Reggiori, F.,
723 van der Laan, M., Frohlich, F., and Ungermann, C. (2018). Vps39 Interacts with Tom40 to Establish One
724 of Two Functionally Distinct Vacuole-Mitochondria Contact Sites. Dev Cell *45*, 621-636 e627.
725 Habersetzer, J., Larrieu, I., Priault, M., Salin, B., Rossignol, R., Brethes, D., and Paumard, P. (2013).
726 Human F1F0 ATP synthase, mitochondrial ultrastructure and OXPHOS impairment: a (super-)complex
727 matter? PLoS One *8*, e75429.
728 Harner, M. (2017). Isolation of Contact Sites Between Inner and Outer Mitochondrial Membranes.
729 Methods Mol Biol *1567*, 43-51.
730 Harner, M., Korner, C., Walther, D., Mokranjac, D., Kaesmacher, J., Welsch, U., Griffith, J., Mann, M.,
731 Reggiori, F., and Neupert, W. (2011). The mitochondrial contact site complex, a determinant of
732 mitochondrial architecture. EMBO J *30*, 4356-4370.
733 Harner, M.E., Unger, A.K., Geerts, W.J., Mari, M., Izawa, T., Stenger, M., Geimer, S., Reggiori, F.,
734 Westermann, B., and Neupert, W. (2016). An evidence based hypothesis on the existence of two
735 pathways of mitochondrial crista formation. Elife *5*.
736 Hoppins, S., Collins, S.R., Cassidy-Stone, A., Hummel, E., Devay, R.M., Lackner, L.L., Westermann, B.,
737 Schuldiner, M., Weissman, J.S., and Nunnari, J. (2011). A mitochondrial-focused genetic interaction
738 map reveals a scaffold-like complex required for inner membrane organization in mitochondria. J Cell
739 Biol *195*, 323-340.
740 Izawa, T., and Unger, A.K. (2017). Isolation of Mitochondria from Saccharomyces cerevisiae. Methods
741 Mol Biol *1567*, 33-42.
742 John Peter, A.T., Herrmann, B., Antunes, D., Rapaport, D., Dimmer, K.S., and Kornmann, B. (2017).
743 Vps13-Mcp1 interact at vacuole-mitochondria interfaces and bypass ER-mitochondria contact sites. J
744 Cell Biol *216*, 3219-3229.
745 Johnson, A., Gin, P., Marbois, B.N., Hsieh, E.J., Wu, M., Barros, M.H., Clarke, C.F., and Tzagoloff, A.
746 (2005). COQ9, a new gene required for the biosynthesis of coenzyme Q in Saccharomyces cerevisiae. J
747 Biol Chem *280*, 31397-31404.
748 Jones, D.T., Taylor, W.R., and Thornton, J.M. (1994). A model recognition approach to the prediction
749 of all-helical membrane protein structure and topology. Biochemistry *33*, 3038-3049.
750 Kemmerer, Z.A., Robinson, K.P., Schmitz, J.M., Manicki, M., Paulson, B.R., Jochem, A., Hutchins, P.D.,
751 Coon, J.J., and Pagliarini, D.J. (2021). UbiB proteins regulate cellular CoQ distribution in Saccharomyces
752 cerevisiae. Nat Commun *12*, 4769.
753 Khosravi, S., and Harner, M.E. (2020). The MICOS complex, a structural element of mitochondria with
754 versatile functions. Biol Chem.
755 Klecker, T., Bockler, S., and Westermann, B. (2014). Making connections: interorganelle contacts
756 orchestrate mitochondrial behavior. Trends Cell Biol *24*, 537-545.
757 Klecker, T., and Westermann, B. (2021). Pathways shaping the mitochondrial inner membrane. Open
758 Biol *11*, 210238.
759 Knop, M., Siegers, K., Pereira, G., Zachariae, W., Winsor, B., Nasmyth, K., and Schiebel, E. (1999).
760 Epitope tagging of yeast genes using a PCR-based strategy: more tags and improved practical routines.
761 Yeast *15*, 963-972.
762 Korner, C., Barrera, M., Dukanovic, J., Eydt, K., Harner, M., Rabl, R., Vogel, F., Rapaport, D., Neupert,
763 W., and Reichert, A.S. (2012). The C-terminal domain of Fcj1 is required for formation of crista junctions
764 and interacts with the TOB/SAM complex in mitochondria. Mol Biol Cell *23*, 2143-2155.
765 Kornmann, B. (2020). The endoplasmic reticulum-mitochondria encounter structure: coordinating lipid
766 metabolism across membranes. Biol Chem *401*, 811-820.
767 Kornmann, B., Currie, E., Collins, S.R., Schuldiner, M., Nunnari, J., Weissman, J.S., and Walter, P. (2009).
768 An ER-mitochondria tethering complex revealed by a synthetic biology screen. Science *325*, 477-481.
769 Kushnirov, V.V. (2000). Rapid and reliable protein extraction from yeast. Yeast *16*, 857-860.
770 Lauffer, S., Mabert, K., Czupalla, C., Pursche, T., Hoflack, B., Rodel, G., and Krause-Buchholz, U. (2012).
771 Saccharomyces cerevisiae porin pore forms complexes with mitochondrial outer membrane proteins
772 Om14p and Om45p. J Biol Chem *287*, 17447-17458.

773 Longtine, M.S., McKenzie, A., 3rd, Demarini, D.J., Shah, N.G., Wach, A., Brachat, A., Philippsen, P., and
774 Pringle, J.R. (1998). Additional modules for versatile and economical PCR-based gene deletion and
775 modification in Saccharomyces cerevisiae. Yeast *14*, 953-961.
776 Macinga, D.R., Cook, G.M., Poole, R.K., and Rather, P.N. (1998). Identification and characterization of
777 aarF, a locus required for production of ubiquinone in Providencia stuartii and Escherichia coli and for
778 expression of 2'-N-acetyltransferase in P. stuartii. J Bacteriol *180*, 128-135.
779 Malinverni, J.C., and Silhavy, T.J. (2009). An ABC transport system that maintains lipid asymmetry in
780 the gram-negative outer membrane. Proc Natl Acad Sci U S A *106*, 8009-8014.
781 Miyata, N., Fujii, S., and Kuge, O. (2018). Porin proteins have critical functions in mitochondrial
782 phospholipid metabolism in yeast. J Biol Chem *293*, 17593-17605.
783 Modi, S., Lopez-Domenech, G., Halff, E.F., Covill-Cooke, C., Ivankovic, D., Melandri, D., Arancibia-
784 Carcamo, I.L., Burden, J.J., Lowe, A.R., and Kittler, J.T. (2019). Miro clusters regulate ER-mitochondria
785 contact sites and link cristae organization to the mitochondrial transport machinery. Nat Commun *10*,
786 4399.
787 Mollet, J., Delahodde, A., Serre, V., Chretien, D., Schlemmer, D., Lombes, A., Boddaert, N., Desguerre,
788 I., de Lonlay, P., de Baulny, H.O*., et al.* (2008). CABC1 gene mutations cause ubiquinone deficiency with
789 cerebellar ataxia and seizures. Am J Hum Genet *82*, 623-630.
790 Morgenstern, M., Stiller, S.B., Lubbert, P., Peikert, C.D., Dannenmaier, S., Drepper, F., Weill, U., Hoss,
791 P., Feuerstein, R., Gebert, M*., et al.* (2017). Definition of a High-Confidence Mitochondrial Proteome
792 at Quantitative Scale. Cell Rep *19*, 2836-2852.
793 Murley, A., Sarsam, R.D., Toulmay, A., Yamada, J., Prinz, W.A., and Nunnari, J. (2015). Ltc1 is an ER-
794 localized sterol transporter and a component of ER-mitochondria and ER-vacuole contacts. J Cell Biol
795 *209*, 539-548.
796 Odendall, F., Backes, S., Tatsuta, T., Weill, U., Schuldiner, M., Langer, T., Herrmann, J.M., Rapaport, D.,
797 and Dimmer, K.S. (2019). The mitochondrial intermembrane space-facing proteins Mcp2 and Tgl2 are
798 involved in yeast lipid metabolism. Mol Biol Cell *30*, 2681-2694.
799 Ozbalci, C., Sachsenheimer, T., and Brugger, B. (2013). Quantitative analysis of cellular lipids by nano-
800 electrospray ionization mass spectrometry. Methods Mol Biol *1033*, 3-20.
801 Papagiannidis, D., Bircham, P.W., Luchtenborg, C., Pajonk, O., Ruffini, G., Brugger, B., and Schuck, S.
802 (2021). Ice2 promotes ER membrane biogenesis in yeast by inhibiting the conserved lipin phosphatase
803 complex. EMBO J *40*, e107958.
804 Paumard, P., Vaillier, J., Coulary, B., Schaeffer, J., Soubannier, V., Mueller, D.M., Brethes, D., di Rago,
805 J.P., and Velours, J. (2002). The ATP synthase is involved in generating mitochondrial cristae
806 morphology. Embo J *21*, 221-230.
807 Phillips, M.J., and Voeltz, G.K. (2016). Structure and function of ER membrane contact sites with other
808 organelles. Nat Rev Mol Cell Biol *17*, 69-82.
809 Poon, W.W., Davis, D.E., Ha, H.T., Jonassen, T., Rather, P.N., and Clarke, C.F. (2000). Identification of
810 Escherichia coli ubiB, a gene required for the first monooxygenase step in ubiquinone biosynthesis. J
811 Bacteriol *182*, 5139-5146.
812 Pu, J., Ha, C.W., Zhang, S., Jung, J.P., Huh, W.K., and Liu, P. (2011). Interactomic study on interaction
813 between lipid droplets and mitochondria. Protein Cell *2*, 487-496.
814 Qian, W., Ma, D., Xiao, C., Wang, Z., and Zhang, J. (2012). The genomic landscape and evolutionary
815 resolution of antagonistic pleiotropy in yeast. Cell Rep *2*, 1399-1410.
816 Rabl, R., Soubannier, V., Scholz, R., Vogel, F., Mendl, N., Vasiljev-Neumeyer, A., Korner, C., Jagasia, R.,
817 Keil, T., Baumeister, W*., et al.* (2009). Formation of cristae and crista junctions in mitochondria depends
818 on antagonism between Fcj1 and Su e/g. J Cell Biol *185*, 1047-1063.
819 Reidenbach, A.G., Kemmerer, Z.A., Aydin, D., Jochem, A., McDevitt, M.T., Hutchins, P.D., Stark, J.L.,
820 Stefely, J.A., Reddy, T., Hebert, A.S*., et al.* (2018). Conserved Lipid and Small-Molecule Modulation of
821 COQ8 Reveals Regulation of the Ancient Kinase-like UbiB Family. Cell Chem Biol *25*, 154-165 e111.
822 Renne, M.F., and Hariri, H. (2021). Lipid Droplet-Organelle Contact Sites as Hubs for Fatty Acid
823 Metabolism, Trafficking, and Metabolic Channeling. Front Cell Dev Biol *9*, 726261.

824 Sakaue, H., Shiota, T., Ishizaka, N., Kawano, S., Tamura, Y., Tan, K.S., Imai, K., Motono, C., Hirokawa, T.,
825 Taki, K.*, et al.* (2019). Porin Associates with Tom22 to Regulate the Mitochondrial Protein Gate
826 Assembly. Mol Cell *73*, 1044-1055 e1048.
827 Schleyer, M., and Neupert, W. (1985). Transport of proteins into mitochondria: translocational
828 intermediates spanning contact sites between outer and inner membranes. Cell *43*, 339-350.
829 Schwaiger, M., Herzog, V., and Neupert, W. (1987). Characterization of translocation contact sites
830 involved in the import of mitochondrial proteins. J Cell Biol *105*, 235-246.
831 Sesaki, H., Dunn, C.D., Iijima, M., Shepard, K.A., Yaffe, M.P., Machamer, C.E., and Jensen, R.E. (2006).
832 Ups1p, a conserved intermembrane space protein, regulates mitochondrial shape and alternative
833 topogenesis of Mgm1p. J Cell Biol *173*, 651-658.
834 Sesaki, H., Southard, S.M., Yaffe, M.P., and Jensen, R.E. (2003). Mgm1p, a dynamin-related GTPase, is
835 essential for fusion of the mitochondrial outer membrane. Mol Biol Cell *14*, 2342-2356.
836 Stefely, J.A., Reidenbach, A.G., Ulbrich, A., Oruganty, K., Floyd, B.J., Jochem, A., Saunders, J.M.,
837 Johnson, I.E., Minogue, C.E., Wrobel, R.L.*, et al.* (2015). Mitochondrial ADCK3 employs an atypical
838 protein kinase-like fold to enable coenzyme Q biosynthesis. Mol Cell *57*, 83-94.
839 Stenger, M., Le, D.T., Klecker, T., and Westermann, B. (2020). Systematic analysis of nuclear gene
840 function in respiratory growth and expression of the mitochondrial genome in S. cerevisiae. Microb
841 Cell *7*, 234-249.
842 Subramanian, K., Jochem, A., Le Vasseur, M., Lewis, S., Paulson, B.R., Reddy, T.R., Russell, J.D., Coon,
843 J.J., Pagliarini, D.J., and Nunnari, J. (2019). Coenzyme Q biosynthetic proteins assemble in a substrate-
844 dependent manner into domains at ER-mitochondria contacts. J Cell Biol *218*, 1353-1369.
845 Tamura, Y., Endo, T., Iijima, M., and Sesaki, H. (2009). Ups1p and Ups2p antagonistically regulate
846 cardiolipin metabolism in mitochondria. J Cell Biol *185*, 1029-1045.
847 Tamura, Y., Kawano, S., and Endo, T. (2019). Organelle contact zones as sites for lipid transfer. J
848 Biochem *165*, 115-123.
849 Tamura, Y., Onguka, O., Hobbs, A.E., Jensen, R.E., Iijima, M., Claypool, S.M., and Sesaki, H. (2012). Role
850 for two conserved intermembrane space proteins, Ups1p and Ups2p, [corrected] in intra-
851 mitochondrial phospholipid trafficking. J Biol Chem *287*, 15205-15218.
852 Tan, T., Ozbalci, C., Brugger, B., Rapaport, D., and Dimmer, K.S. (2013). Mcp1 and Mcp2, two novel
853 proteins involved in mitochondrial lipid homeostasis. J Cell Sci *126*, 3563-3574.
854 Thong, S., Ercan, B., Torta, F., Fong, Z.Y., Wong, H.Y., Wenk, M.R., and Chng, S.S. (2016). Defining key
855 roles for auxiliary proteins in an ABC transporter that maintains bacterial outer membrane lipid
856 asymmetry. Elife *5*.
857 Unger, A.K., Geimer, S., Harner, M., Neupert, W., and Westermann, B. (2017). Analysis of Yeast
858 Mitochondria by Electron Microscopy. Methods Mol Biol *1567*, 293-314.
859 von der Malsburg, K., Muller, J.M., Bohnert, M., Oeljeklaus, S., Kwiatkowska, P., Becker, T., Loniewska-
860 Lwowska, A., Wiese, S., Rao, S., Milenkovic, D.*, et al.* (2011). Dual role of mitofilin in mitochondrial
861 membrane organization and protein biogenesis. Dev Cell *21*, 694-707.
862 Wenz, L.S., Opalinski, L., Schuler, M.H., Ellenrieder, L., Ieva, R., Bottinger, L., Qiu, J., van der Laan, M.,
863 Wiedemann, N., Guiard, B.*, et al.* (2014). The presequence pathway is involved in protein sorting to
864 the mitochondrial outer membrane. EMBO Rep *15*, 678-685.
865 Westermann, B., and Neupert, W. (2000). Mitochondria-targeted green fluorescent proteins:
866 convenient tools for the study of organelle biogenesis in Saccharomyces cerevisiae. Yeast *16*, 1421-
867 1427.
868 Wittig, I., Braun, H.P., and Schagger, H. (2006). Blue native PAGE. Nat Protoc *1*, 418-428.
869 Wong, E.D., Wagner, J.A., Scott, S.V., Okreglak, V., Holewinske, T.J., Cassidy-Stone, A., and Nunnari, J.
870 (2003). The intramitochondrial dynamin-related GTPase, Mgm1p, is a component of a protein complex
871 that mediates mitochondrial fusion. J Cell Biol *160*, 303-311.
872 Xie, J., Marusich, M.F., Souda, P., Whitelegge, J., and Capaldi, R.A. (2007). The mitochondrial inner
873 membrane protein mitofilin exists as a complex with SAM50, metaxins 1 and 2, coiled-coil-helix coiled-
874 coil-helix domain-containing protein 3 and 6 and DnaJC11. FEBS Lett *581*, 3545-3549.

875 Xie, L.X., Ozeir, M., Tang, J.Y., Chen, J.Y., Jaquinod, S.K., Fontecave, M., Clarke, C.F., and Pierrel, F.
876 (2012). Overexpression of the Coq8 kinase in Saccharomyces cerevisiae coq null mutants allows for
877 accumulation of diagnostic intermediates of the coenzyme Q6 biosynthetic pathway. J Biol Chem *287*,
878 23571-23581.
879 Zerbes, R.M., Bohnert, M., Stroud, D.A., von der Malsburg, K., Kram, A., Oeljeklaus, S., Warscheid, B.,
880 Becker, T., Wiedemann, N., Veenhuis, M.*, et al.* (2012). Role of MINOS in mitochondrial membrane
881 architecture: cristae morphology and outer membrane interactions differentially depend on mitofilin
882 domains. J Mol Biol *422*, 183-191.
883 Zick, M., Duvezin-Caubet, S., Schafer, A., Vogel, F., Neupert, W., and Reichert, A.S. (2009). Distinct roles
884 of the two isoforms of the dynamin-like GTPase Mgm1 in mitochondrial fusion. FEBS Lett *583*, 2237-
885 2243.

886